Lab on a Chip

ROYAL SOCIETY OF CHEMISTRY

TUTORIAL REVIEW

View Article Online
View Journal

Check for updates

Cite this: DOI: 10.1039/d5lc00628g

Flow by design: a guided review of microfluidics for wearable biosensors

Julieta Nava-Granados,[a] Katherine Vasquez,[ab] Bryan U. Medina,[b] Catherine Wang,[a] Jose R. Moreto[a] and Juliane Sempionatto*[a]

Received 24th June 2025,
Accepted 16th September 2025

DOI: 10.1039/d5lc00628g

rsc.li/loc

The integration of microfluidics into wearable biosensors has enabled real-time, non-invasive access to physiological information through biofluids such as sweat, saliva, tears, and interstitial fluid (ISF). However, the successful design and fabrication of microfluidic systems for wearables requires interdisciplinary expertise in fluid dynamics, materials science, microfabrication, and device integration. These significant barriers can hinder rapid innovation and adoption. This review aims to serve as a guide for researchers and engineers developing microfluidic systems for wearable applications. We provide a step-by-step overview of microfluidic design principles, material selection, fabrication methods, and strategies for fluid handling and sampling. Attention is given to the constraints and opportunities unique to wearable formats, such as flexibility, biocompatibility, and integration with sensors and electronics. We also highlight future trends in the field, including the integration with artificial intelligence (AI), design automation, and novel flow control technologies. By providing clear guidance on the design and implementation process, this review seeks to accelerate the development of microfluidic platforms for continuous health monitoring.

Introduction

Microfluidic systems are revolutionizing the field of non-invasive monitoring by enabling continuous sampling and real-time analysis of biofluids such as sweat, saliva, tears, and ISF directly from the body (Fig. 1a). The development of such wearable systems could eliminate the need for traditional lab-based diagnostics, which can be costly, time-consuming, labour-intensive, and require trained personnel.[1] At the core of these systems are microfluidic biosensors, which use a combination of microfluidic chips to collect and analyse biofluids, integrating detection, signal control, and data output in a single system.[2] When built in a wearable format, these biosensors allow for

---

[a] *Department of Electrical and Computer Engineering, Rice University, Houston, TX 77005, USA. E-mail: jsemp@rice.edu*
[b] *Department of Bioengineering, Rice University, Houston, TX 77005, USA*

Julieta Nava-Granados

Julieta Nava-Granados is a PhD student in the Electrical and Computer Engineering Department at Rice University and a Fulbright-García Robles Scholar. Her background spans nanosatellite design, IC design, mechatronics, robotics, and microelectronics, reflecting a diverse technical foundation. She is interested in developing cutting-edge wearable biosensors with a focus on advancing women's health. Beyond her work, she is committed to advocating for inclusivity and inspiring women to pursue careers in STEM.

Katherine Vasquez

Katherine Vasquez is a Bioengineering PhD student at Rice University. Her experience spans neuroscience, user experience design, and vaccine engineering. She has studied how neurons in the auditory cortex localize sound, built a mobile app that immerses people in the music and history of jazz in New York City, and advanced a DNA-based vaccine platform for broad protection against Streptococcus pneumoniae. Now, she is focused on creating low-cost wearable technologies to predict, prevent, and monitor health challenges tied to organ transplantation, immune health, cardiovascular disease, and mental well-being.

continuous, real-time sampling and non-invasive health monitoring.

Microfluidic biosensors are defined by two fundamental technological components: the microfluidic and the biosensing technology.[3] Microfluidic chips operate by unique properties of fluid dynamics at the microscale, which differ significantly from fluid dynamics at the macroscale. Microfluidic flow is characterized by a low Reynolds number, indicating that the flow is laminar (smooth) rather than turbulent. This is because inertial forces are negligible at the microscale, meaning that fluid momentum has a minimal effect on flow behavior. Instead, viscous forces predominate, resulting in a laminar flow that can be manipulated and collected in micro-volumes *via* microchannels.[4] Collected fluids can then be transported to the biosensing sites, where biomolecules present in the fluid bind to specific biorecognition elements. This binding process can produce electrochemical, electrical, optical, acoustic, or magnetic signals that can be transduced and measured by an external reader.[5]

Bryan U. Medina

Bryan U. Medina is a senior Bioengineering student at Rice University, where he leads the SimplySpiro project, which focuses on developing a non-invasive respiratory monitoring device that integrates custom sensors, low-noise amplifiers, and wireless analytics. Previously, Bryan conducted research at Baylor College of Medicine on a closed-loop robotic instrumentation system designed to study the neural circuits of breathing. In addition, Bryan has completed internships at Rice University, Stanford University, the University of Houston, and Boston University, contributing to projects in microfluidic biosensors, bioinformatics, medical device prototyping, and clinical health outcomes.

Catherine Wang

Catherine Wang is an undergraduate student in the Department of Electrical and Computer Engineering at Rice University. She is currently an undergraduate researcher in the Sempionatto Lab, where she assists in the design and development of wearable biomedical devices. Her research interests include wearable and implantable platforms for continuous health monitoring, early disease detection, and predictive diagnostics. She is also interested in medical and surgical robotics, as well as the broader applications of engineering in medicine and healthcare.

Jose Roberto Moreto

Dr. Jose Roberto Moreto is an Assistant Teaching Professor in the Department of Electrical and Computer Engineering at Rice University. He specializes in experimental fluid mechanics, turbulence characterization, and advanced flow diagnostics using particle image velocimetry (PIV) and pressure reconstruction techniques. He has extensive experience in aerodynamics, water tunnel instrumentation, and turbulence modeling with applications in aerospace, energy, and environmental systems. Previously, he worked as an Aerodynamics Engineer at Aeromutable and a Product Development Engineer at Embraer S.A. Dr. Moreto earned his Ph.D. in Engineering Sciences from the San Diego State University/UC San Diego Joint Doctoral Program and a B.Sc. in Aeronautical Engineering from the University of São Paulo.

Juliane R. Sempionatto

Dr. Juliane R. Sempionatto is an Assistant Professor holding the James J. Truchard endowed chair in the Electrical and Computer Engineering Department at Rice University, affiliated with the Digital Health Initiative. She specializes in developing advanced wearable biosensors designed for continuous, real-time monitoring of health biomarkers in sweat, saliva, tears, interstitial fluid, and blood. Her research leverages electrochemical sensors, soft electronics, microfluidics, and machine learning to enable personalized healthcare, early disease detection, and therapeutic monitoring. Previously, Dr. Sempionatto was a postdoctoral researcher at Caltech and completed her Ph.D. in Nanoengineering at UC San Diego. Recognized internationally, she is a recipient of several prestigious awards, including the Siebel Scholar, MIT Innovators under 35 (Latin America), IUPAC Young Chemist Award, and ScientistA.

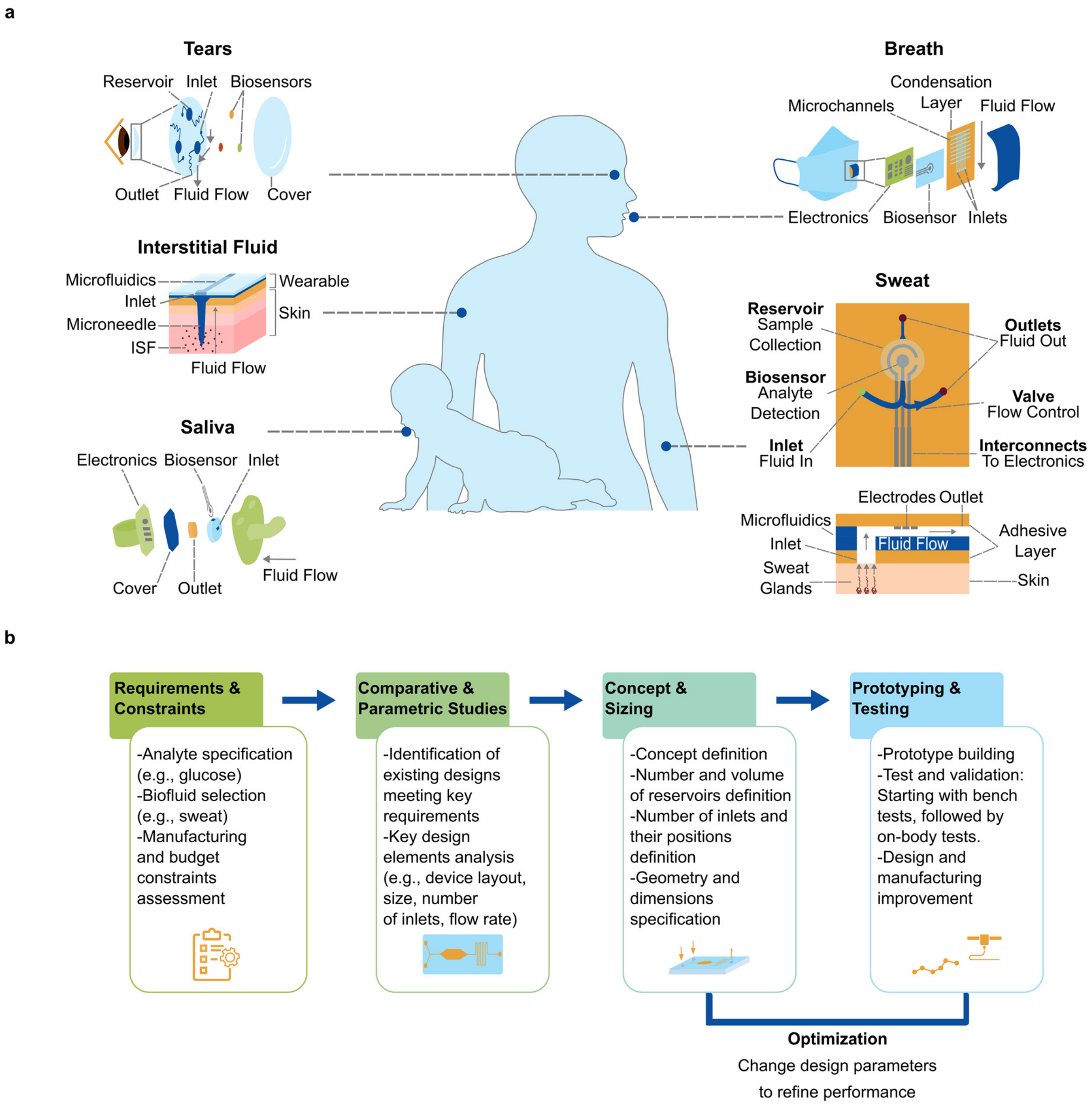

Fig. 1 Microfluidics for wearable sensors. a) Microfluidics for biofluids: tears, saliva, breath, interstitial fluid (ISF), and sweat. The schematic shows the basic components of microfluidics for wearable biosensors. Inlets allow the fluid to flow into the system. Valves and pumps control the flow. The reservoir and biosensor facilitate sample collection and analyte detection. Interconnects enable interfacing with external electronics, and outlets permit fluid exit from the system. b) Overview of the microfluidic design process. From the requirements and constraints, study of existing designs, microfluidic layout design, prototyping, and testing.

The performance of microfluidic sensors depends on several design parameters. The geometry and width of microchannels can affect the velocity field, shear stress, and pressure distribution, influencing flow behavior within the microfluidic device.[6] Material selection for chip fabrication is also a critical design decision, as the surface properties, rigidity, and elasticity of the material can significantly affect fluid behavior.[7] Beyond the standard design parameters for designing and fabricating a microfluidic system, wearable applications introduce several other key constraints, as wearable microfluidic sensors ideally conform to the skin, are biocompatible, lightweight, user-friendly, and operate with minimal power requirements.[8,9]

While several reviews have addressed the applications of wearable microfluidics for health monitoring, a notable gap remains in the literature regarding the engineering principles required to design and fabricate custom microfluidic systems. Existing reviews often focus on summarizing devices or specific biofluid applications,[10–13] but they seldom provide practical guidance on how to translate fundamental microfluidic concepts into functional wearable platforms. Moreover, many of the proposed microfluidics for wearable systems present only minor variations or copies of previous designs, often without optimization of new architectures for specific sensing needs. Thus, increasingly challenging for researchers and engineers new to the field to develop tailored solutions that meet the unique demands of wearable biosensing.

This review is structured to guide the reader from fundamental principles to advanced strategies in wearable microfluidics based on engineered microchannels. It is important to note that while other fluidic systems, such as paper-based ones, have proven highly valuable for point-of-care and disposable diagnostics, a comprehensive theoretical treatment of these systems, including governing equations such as Washburn-type capillary flow and their associated design constraints[14] would require a dedicated review.[15–18] Accordingly, this article focuses on engineered wearable microchannels, which present a distinct set of challenges and opportunities. Our objective is to provide a tutorial-style resource that equips researchers with design strategies, fabrication methods, and system-integration principles tailored to wearable applications.

The organization of this review is so that it progressively builds the reader's understanding of wearable microfluidic systems, moving from theoretical fundamentals to practical implementation. The text begins with the basics of microfluidics and fluid handling, followed by a design case study, design requirements and constraints, and lastly with material selection and fabrication methods. We also highlight the field's future trends and directions, from design automation and new fabrication techniques to the use of novel biofluids. Furthermore, we created a Jupyter Notebook available on Google Colab to guide researchers through the initial design of wearable microfluids. In this Notebook, the user enters the biofluid and the materials desired for the device, and the initial dimensions and other fluid mechanics properties are calculated. The objective of this review is to provide a guide for designing microfluidics for newcomers, scientists, scholars, and enthusiasts interested in the field of wearable biosensors (Fig. 1b).

Historical context of wearable microfluidic systems

Microfluidics emerged in the 1990s as a miniaturized approach to chemical analysis, laying the groundwork for modern lab-on-a-chip devices. A seminal 1993 Science paper by Harrison *et al.* is often credited with establishing microfluidics as a distinct research field,[19] following the earlier μTAS (micro total analysis system) concept proposed by Manz and coworkers in 1990.[20] Throughout the 1990s and 2000s, advances such as soft lithography by Whitesides and colleagues (*e.g.*, PDMS-based microchannels) greatly expanded microfluidic device fabrication.[21] These developments enabled complex microchannel networks and on-chip assays that became ubiquitous in analytical chemistry and biology labs. By the early 2010s, researchers began exploring how to bring microfluidic technology out of the laboratory and onto the body, aiming for real-time monitoring of biofluids such as sweat outside of controlled settings.

Sweat attracted interest as an accessible biofluid rich in biomarkers.[22] Early wearable sweat sensors were relatively simple and often focused on single analytes. For example, Diamond's group demonstrated a wearable electrochemical patch for real-time sweat sodium measurement as early as 2010.[23] In 2013, Joseph Wang's team introduced "electronic tattoo" sensors for lactate in sweat,[24] illustrating the potential of printed flexible electronics for non-invasive monitoring. European efforts like the BIOTEX project also integrated microfluidics into textiles around 2010,[25] and others explored adhesive patches with wireless readout (*e.g.*, an RFID-based sweat electrolyte patch in 2015).[26]

One of the major turning points for wearable microfluidics came with the first report of a soft, skin-mounted microfluidic system that truly functioned as "labs on the skin". John A. Rogers and colleagues developed two pivotal contributions to the field. In 2014, they reported an ultrathin sweat sensor built on microporous elastomeric substrates for spontaneous collection of sweat *via* capillary forces.[27] Two years later, Roger's group developed a thin, stretchable microfluidic patch that adheres to skin and routes sweat through a network of channels and micrometer-scale reservoirs.[28] This device, published in 2016, enabled *in situ* colorimetric analysis of multiple sweat biomarkers (glucose, lactate, chloride, pH) without the need for bulky equipment. Around the same time, Ali Javey's group reported a fully integrated sensor array for multiplexed perspiration analysis.[22] Their system incorporated on-board electronics to simultaneously measure sweat metabolites and electrolytes in real time, contributing significantly to the advances in the sensing aspect of wearables. These breakthroughs demonstrated the power of combining microfluidic sample handling with wearable electronics, achieving on-body chemical analysis that was previously possible only in the laboratory.

Since 2016, the field of epidermal microfluidics has grown rapidly, led by a few key groups often working collaboratively across disciplines.[9,29–32] Rogers' group has continued to pioneer skin-interfaced microfluidic platforms, for example, developing patches with capillary bursting valves to measure sweat gland pressures[33] and battery-free wireless sweat sensors that integrate microfluidics with electronics.[34] In 2020, a microfluidic sweat patch was tested on hundreds of athletes, showing strong correlations between patch-readouts and whole-body hydration metrics.[35] Such studies underscore how far technology has come from the early absorbent-pad methods. In summary, what began as micro-scale plumbing for lab assays has evolved into fully epidermal microfluidic systems. Pioneering contributions have converged to bring lab-on-a-chip functionality to the surface of the skin. The result is a new class of bio-integrated devices that combine the analytical sophistication of microfluidics with the convenience of wearable tech, enabling continuous, non-invasive insight into human physiology.

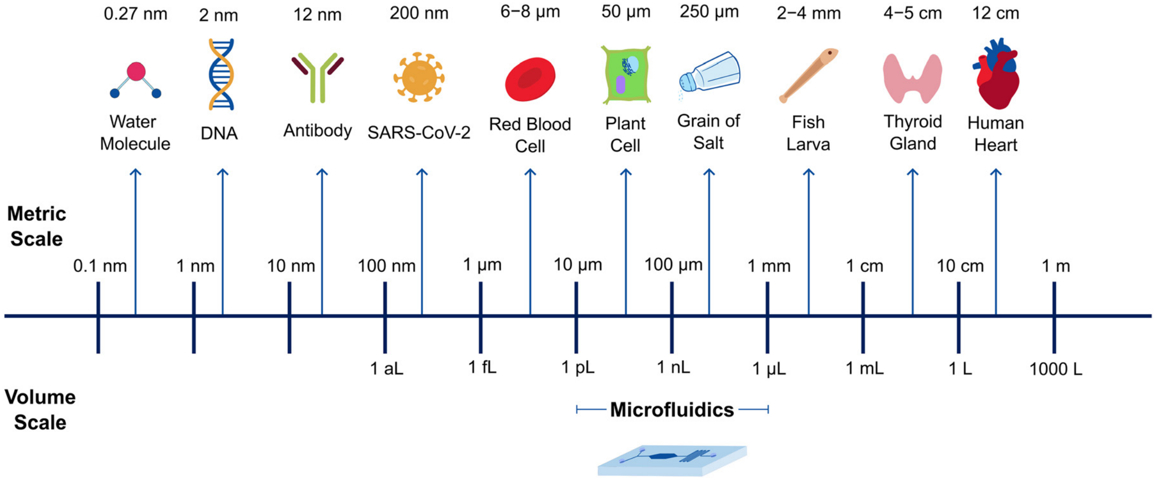

Fig. 2 Size comparison between the microfluidic volumetric scale and length scale. The figure shows how small volumes sampled by microfluidic devices compare to common objects in nature.

Fundamentals of microfluidics for sensing

Fluid transport in microfluidic devices is typically achieved through two main architectures: passive flow in porous substrates (such as paper) and controlled flow in engineered microchannels. Paper-based systems rely on spontaneous wicking through random pore networks, which makes them attractive for low-cost, disposable diagnostics where simplicity and affordability are critical. In contrast, engineered microchannels enable precise control over geometry, surface chemistry, and flow dynamics, capabilities that are essential for wearable applications demanding continuous operation, mechanical robustness, and seamless integration with sensing and electronic components. In this review, we focus on the fundamental principles of engineered microchannels, which define the design space for wearable biosensing platforms. For readers seeking a deeper treatment of paper-based microfluidics for diagnostics and sensing, comprehensive discussions can be found in several recent reviews.[15–18]

Microfluidic systems typically involve sampling volumes in the picoliter to microliter range,[36,37] using microchannels with at least one dimension below 1 mm (ref. 38) (Fig. 2). At this scale, fluid behavior differs significantly from the macroscale. The first step to determining such behavior is to calculate which forces, such as fluid viscosity, surface tension, and gravity, dominate fluid motion within the channels. To this end, there are comprehensive and complete sets of fluid-dynamic equations that can model the flow dynamics, such as the Navier–Stokes equations.[36,39]

However, directly solving these equations for every new geometry or material combination can be extremely complex. Alternatively, dimensional analysis offers a systematic way to reduce complexity by grouping variables into dimensionless numbers that compare the relative magnitudes of competing effects. While this method does not provide an optimal solution, it is extremely useful for preliminary design.[39–41] By evaluating the order of magnitude of specific dimensionless groups (Table 1), it is possible to predict whether the flow will be laminar (smooth) or turbulent, and if it will be affected by capillarity or significantly influenced by gravity, without detailed simulations or experiments for each design variant.[4]

Table 1 shows important selected dimensionless groups (not comprehensive) used for studying the flow properties in a

Table 1 Common variables and selected dimensionless groups for flow analysis in a microchannel. Adapted from ref. 45. Sweat fluid properties and order of magnitude are based on water (ρ = 1000 kg m^{-3}, μ = 1.0 mPa s, σ = 72 mN m^{-1}) flowing with velocity V = 1 mm s^{-1} in a microchannel (L = 100 μm)

Name	Dimensionless group	Interpretation	Order of magnitude in the sweat microchannel
Reynolds, Re	$\frac{\rho VL}{\mu}$	$\frac{\text{Inertia Force}}{\text{Viscous Force}}$	1.0×10^{-2}; Re $\ll 1$; flow is laminar, and inertia is negligible. Viscous force dominates
Weber, We	$\frac{\rho V^2 L}{\sigma}$	$\frac{\text{Inertia Force}}{\text{Surface Tension Force}}$	1.4×10^{-6}; We $\ll 1$; inertial forces are negligible compared with surface tension forces
Capillary, Ca	$\frac{\mu V}{\sigma}$	$\frac{\text{Viscous Force}}{\text{Surface Tension Force}}$	1.4×10^{-5}; Ca $\ll 1$; surface tension forces are important
Bond, Bo	$\frac{\Delta\rho g L^2}{\sigma}$	$\frac{\text{Gravitational Force}}{\text{Surface Tension Force}}$	1.4×10^{-3}; Bo $\ll 1$; gravitational forces are negligible, and surface tension forces dominate
Peclet, Pe	$\frac{VL}{D}$	$\frac{\text{Convection}}{\text{Diffusion}}$	1.7×10^{2}; Pe $\gg 1$; in microchannels, bulk flow typically delivers analytes to the sensor faster than diffusion, significantly affecting the sensor's response time

Table 2 Parametric study. This table summarizes key microfluidic design and performance parameters for biosensors developed for various biofluids, including tear fluid, ISF, saliva, and sweat. Devices are compared based on temporal resolution, flow characteristics, reservoir and inlet geometry, channel dimensions, flow mechanisms, fluidics material, fabrication methods, and references

Biofluid	Temporal resolution	Refresh time/flow rate	System geometrical parameters	Flow mechanism	Fluidics material and fabrication	Dimensionless numbers
Tear[56]	Single point (30 s readout)	2 s infiltration 30 s reaction time	Reservoir volume: ~20 μL Reservoir Ø: 4 mm Inlet dimensions: 25 × 4 mm Channel: 8 × 2 mm	Capillary	Filter paper, wax, adhesives Laminates, wax patterning	Re: 3.28×10^{-2} Ca: 1.5×10^{-5} Bo: 8.92×10^{-1} Pe: 5.2×10^{3}
Tear[57]	1 min (color stabilizes)	~4 s to fill 60 s for 90% of concentration	Reservoir volume: ~22.6 μL Channel: 800 × 800 μm	Gravity-driven	PDMS, adhesives Soft lithography, plasma treatment	Re: 1.11×10^{0} Ca: 1.28×10^{-3} Bo: 1.43×10^{-2} Pe: 1.77×10^{5}
ISF[58]	Collection within 1 minute	~0.014 μL per pore <1 μL total	Inlet dimensions: 100 × 100 μm Channel: 50 × 40 μm	Capillary	PDMS, polyimide, adhesives Soft lithography, plasma treatment	Re: 1.48×10^{-3} Ca: 5.61×10^{-6} Bo: 2.66×10^{-4} Pe: 1.30×10^{2}
ISF[59]	On-demand	~26 s R6G appearance ~136 s full channel fill ~0.8 μL min^{-1}	Reservoir volume: 1.8 μL Inlet area: ~0.2 cm^{2} Channel width: 150 μm	Capillary Manual suction	PDMS, polyimide, adhesives Soft lithography, plasma treatment, and laminates	Re: 2.02×10^{-3} Ca: 2.27×10^{-6} Bo: 3.03×10^{-3} Pe: 1.77×10^{2}
Saliva[60]	~50 min per reading	Self-driven cycle Entire chip: ~50 min	Reservoir volume: ~0.3–0.5 μL Reservoir Ø: 0.85 mm Mixing channel: 3 mm Outlet: 0.2 × 0.1 mm	Capillary Microvalves Pumping	PMMA, PDMS CNC engraving, laminates	Re: 3.83×10^{-3} Ca: 3.42×10^{-6} Bo: 3.05×10^{-3} Pe: 2.50×10^{2}
Sweat, ISF[55]	Minutes to hours	Sweat: 0.07–5 μL min^{-1} cm^{-2} ISF: nL–μL min^{-1}	Reservoir volume: 5–100 μL Inlet area: 0.2–7 cm^{2} Channel dimensions: width: 100–1000 μm Height: 50–300 μm Length: 1–10 cm	Capillary Osmosis Evaporation	PMMA, PET, PDMS, paper, thread wicks, hydrogels, adhesives Soft lithography, laser cutting, 3D printing, laminates	Re: 1.06×10^{-6}, 5.34×10^{2} Ca: 2.67×10^{-9}, 1.64×10^{-3} Bo: 5.99×10^{-4}, 2.91×10^{-2} Pe: 1.00×10^{-1}, 1.35×10^{-6}
Sweat[28]	~5 min	0.3–3.2 h to fill (1.2–12 μL h^{-1}) Linear: 0.07–0.7 mm min^{-1}	Reservoir volume: ~5–10 μL Inlets Ø: 3 mm Inlet area: ~10 glands ≈ 0.07 cm^{2} Channel: 100 μm wide × 2.5 mm long	Capillary	PDMS, adhesives Soft lithography, plasma treatment, and laminates	Re: 1.74×10^{-3} Ca: 1.64×10^{-7} Bo: 3.07×10^{-3} Pe: 4.38×10^{4}
Sweat[47]	Real-time Sub-minute after filling	Fill time: ~13.4 min ~0.68 μL min^{-1}	Reservoir volume: ~8.24–8.72 μL Reservoir Ø: 5 mm Inlet area: ~0.0154 cm^{2} Channel height: 300 μm	Capillary	PDMS, adhesives Soft lithography, plasma treatment, and laminates	Re: 4.36×10^{-2} Ca: 2.57×10^{-6} Bo: 7.87×10^{-3} Pe: 1.10×10^{3}
Sweat[61]	4–20 s (50 μL min^{-1}) 2–9 min (2 μL min^{-1}) <20 s for levodopa	Detectable at 2 nL min^{-1} <3 min at 300 nL min^{-1} cm^{-2} <30 s at 3 μL min^{-1} cm^{-2}	Reservoir volume: ~200 nL (with filter) ~750 nL total Wells Ø: 3–10 mm Channel: 70 × 70 μm and 200 × 70 μm ~15 cm spiraling length	Capillary Wettability	PET, PDMS, hydrogels, adhesives Soft lithography, chemical surface treatment, and laminates	Re: 1.18×10^{-2} Ca: 2.39×10^{-6} Bo: 6.69×10^{-4} Pe: 2.98×10^{2}

PMMA – polymethyl methacrylate; PDMS – polydimethylsiloxane; PET – polyethylene terephthalate.

microchannel. These groups are based on the most relevant parameters for microchannel flow: channel reference length (L), flow velocity (V), fluid density (ρ), fluid viscosity (μ), surface tension (σ), diffusivity (D), and the gravitational acceleration (g). Moreover, Table 1 presents the order of magnitude of each group for sweat flowing in a microchannel.

For example, for sweat flowing with a velocity V = 1 mm s^{-1} in a microchannel with dimensions x and y, the order of magnitude of these dimensionless groups indicates that viscous forces (internal friction in the fluid due to viscosity) and capillary forces (surface tension at the liquid–air or liquid–solid interface) dominate on the microchannel scales. While gravity forces (force exerted by gravity) and inertial forces (which are associated with the fluid's resistance to changes in its motion due to its mass) can be neglected. Since viscous and capillary forces are predominant at the micro scale, their influence on microchannel fluid flow will be examined in the following discussion, starting with the implications of low Reynolds number magnitude regimes.

For sweat-sensor microchannels, the Reynolds number (Re – the ratio of inertial forces to viscous forces) is typically below 1 (see Table 2 and ref. 38). This indicates that viscosity dominates with respect to inertial forces. In this regime, flow tends to be laminar, smooth, and stable with low mixing, as opposed to turbulent, where flow is more chaotic with swirls and high mixing. This smooth flow regime simplifies the design due to the already existing analytical models.[4,42–44] We will explore the concept with a case study later in the review.

Another key parameter in microchannel fluid dynamics is capillary forces, which are of similar magnitude to viscous forces. This relationship is captured by the Capillary number (Ca), which is defined as the ratio of viscous forces to surface tension forces. In typical sweat microchannels, Ca $\ll$ 1 (Table 2), indicating that surface tension is a major contributor to flow behavior. In practical terms, this means that narrower channels generate higher capillary pressure, enabling flow in hydrophilic surfaces. However, they restrict the flow in hydrophobic channels, where flow may be reduced or even blocked. For longer or wider channels, viscous pressure losses become the dominant resistance to flow.[4,36,39,40,42]

On the other hand, gravitational effects are negligible at the microscale.[4,39] The Bond number (Bo) is used to compare gravitational forces to surface tension forces, and it is typically very small in microfluidic devices (Table 2). This means that gravity has minimal influence on how the fluid moves through the microchannels.[38,39,42] As a result, the orientation of the device (whether vertical, horizontal, or upside down) has little impact on flow, provided that the microfluidic device walls remain wetted. This characteristic is particularly important for wearable devices, which must operate reliably regardless of body position or movement.

The non-dependency on orientation ensures consistent performance under a wide range of real-life conditions, making microfluidic devices well-suited for wearable applications.

The last relevant dimensionless number is the Peclet number (Pe). Unlike the other groups, it is not a ratio of forces, but rather a ratio of transport rates. Specifically, it is the rate of convective transport to diffusive transport.[4] In high-Pe conditions, advection dominates over diffusion, meaning that analytes are primarily transported by bulk flow rather than by molecular diffusion.[4,39,46] When high-Pe conditions coincide with low-Re conditions, there are important implications for sensor performance: fresh fluid must feed the sensor surface continuously to maintain time resolution while avoiding cumulative effects.[36] Without sufficient flow, analytes may accumulate near the sensor, leading to signal saturation and misreadings. In microfluidic systems, the combination of high Peclet and low Reynolds numbers must be carefully considered during the design process to ensure reliable and responsive sensing.

It is important to notice that while dimensional analysis provides a robust foundation for understanding the governing forces in fluid flows,[40–42,45] it only provides a preliminary, theoretical overview of the microchannel's performance. Real-world operating conditions often introduce deviations from the idealized assumptions of steady flow and full channel wetting. Body motion can generate transient pressure fluctuations, sweat production can vary dynamically, and incomplete wetting of microchannels can disrupt predicted flow behavior. These practical challenges highlight the importance of incorporating design tolerances, such as redundant fluidic pathways, flexible substrates that absorb motion-induced disturbances, flow rate sensors, and signal processing to filter motion background noise. Such strategies extend the utility of first-order analysis into the realities of wearable operation, bridging the gap between theory and practice.

With this in mind, we will now apply the theoretical insights from dimensional analysis to engineer the preliminary design a wearable microfluidic system. Having identified through dimensional analysis that viscous and capillary forces govern the flow dynamics, while gravitational and inertial forces are negligible, it is possible to translate these insights into a preliminary microfluidic design. The general objective of this microfluidic system is to maintain a continuous and stable flow of sweat across the sensing interface, ensuring accurate real-time measurements of analyte concentrations.

To do so, a key starting point in the design process is the geometry of the sensor itself. Sensor dimensions depend on the target analyte, detection technique, and the chosen fabrication method. For example, Gao *et al.* (2016) selected a 3 mm diameter electrochemical biosensor to detect low concentrations of glucose in sweat, obtaining a high current response.[22] Therefore, the microfluidic system must physically accommodate the sensor, typically through a reservoir whose footprint matches or slightly exceeds that of the sensor. To minimize dead volume (fluid that does not contribute to sensing), this reservoir should be as compact as possible. In early-stage design, the channel and reservoir geometries are often assumed to be rigid, but material flexibility may later be considered during mechanical or functional optimization, once large flexible/soft reservoirs might collapse over the sensor.

Reservoir shape significantly affects performance (Fig. 3). The device shown in Fig. 3c(i) features a geometry that closely matches the footprint of the sensor, effectively minimizing dead volume. In contrast, the design in Fig. 3c(ii) uses a rectangular reservoir that significantly exceeds the sensor's width, resulting in substantial dead volume. In this configuration, much of the incoming fluid flows into regions not covered by the sensor, which reduces analyte replenishment at the sensing surface. As a result, sensor readings may become less responsive to real-time changes in analyte concentration.

Once the reservoir geometry is defined, the minimum volume required to fill it can be estimated. The operational flow rate can be calculated to reduce both the time needed to fill the reservoir and the average flow rate required to maintain fluid replenishment, which are determined by the application and the characteristics of the sensor. The sampling inlet area must be sufficient to collect the volume of sweat necessary to fill the reservoir within the desired time interval, and to provide the operational flow rate. In many

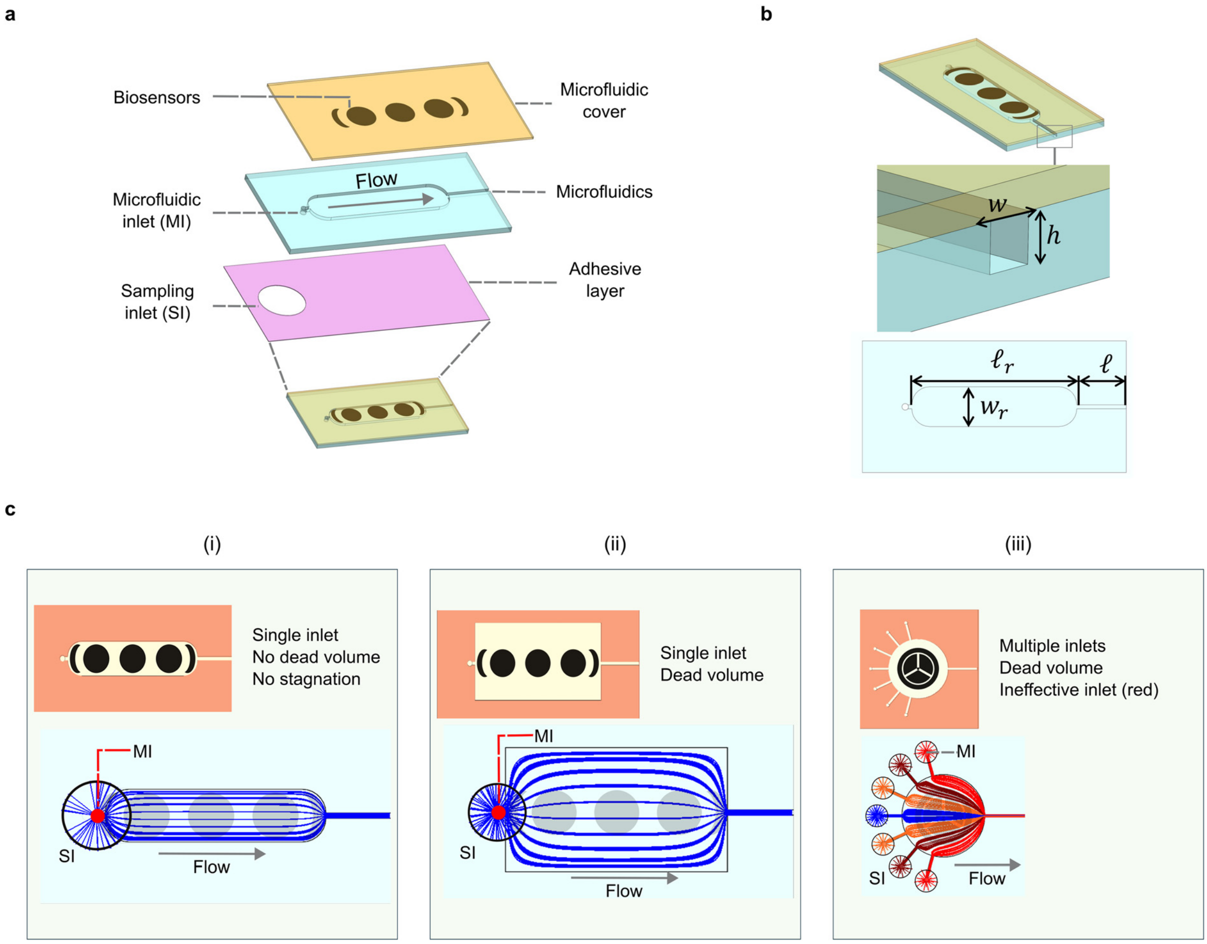

Fig. 3 Wearable microfluidic device for sweat collection and sensing. a) Exploded view of the device. The bottom adhesive layer attaches the device to the skin and contains at least one sampling inlet (SI) to collect sweat. The microfluidic layer, typically made of a flexible material such as PDMS, contains the microfluidic inlet (MI) that receives the collected sweat from the SI. This layer includes channels that guide fluid to the reservoir, where sensors are located. From the reservoir, sweat is guided outside the device by the outlet channel. The top layer is the microfluidic cover containing the biosensor (printed electrode). b) Key geometric parameters. The reservoir has a length ℓ_r, width w, and height h; the outlet channel has a length ℓ, width w, and shares the same height h. Typically, all the microfluidics components have the same height due to manufacturing constraints. The system may include multiple sampling inlets, reservoirs, and microchannels, depending on the design. c) Laminar flow streamlines for three device configurations: (i) a single inlet and outlet aligned on opposite ends of a compact reservoir that closely matches the sensor footprint. This design minimises dead volume and ensures that incoming fluid passes directly over the sensor surface. (ii) A similar single-inlet/outlet layout but with an oversized reservoir. A significant portion of the fluid does not flow over the sensor, resulting in increased dead volume and reduced sensing efficiency, and increasing the time to fill up the reservoir. (iii) A configuration with multiple sampling inlets connected to the reservoir through short microchannels. In some designs, multiple inlets are necessary to ensure sufficient sweat collection from a large skin area. However, this introduces trade-offs between minimizing the length of the connecting channels and optimizing the reservoir inlet locations relative to the outlet. In this example, only the inlet positioned directly opposite the outlet (blue streamlines) effectively directs fluid across the sensor surface. Inlets located closer to the outlet (red streamlines) contribute minimally, with fluid bypassing the sensing region. This highlights the importance of carefully balancing inlet placement and channel routing to achieve efficient analyte delivery.

cases, a single inlet may not be practical. Depending on the flexibility of the materials used, a large inlet may deform under stress, increasing dead volume and reducing structural integrity. On another hand, if the sampling inlets are too small, they may not align with active sweat glands, limiting fluid uptake. Therefore, several sampling inlets may be needed, and they should be appropriately sized and positioned to ensure effective sweat collection.

In general, sampling inlets should be placed as close as possible to the reservoir to minimize the length of the connecting microchannels. Longer channels contribute to increased dead volume and time required to fill the system. Because flow in these systems is typically laminar, the microfluidic inlets should direct fluid toward a single-entry point on one side of the reservoir, while the outlet should be placed on the opposite side. This layout ensures consistent fluid movement across the sensor surface, enhancing analyte replenishment.

The effect of inlet placement is illustrated in Fig. 3. In Fig. 3c(i), a single microfluidic inlet and outlet are located on opposite sides of the reservoir, directing fluid across the sensor and promoting effective analyte transport. On another hand, in Fig. 3c(iii), multiple sampling inlets are used. The inlets directly across from the outlet contribute most to replenishing the flow over the sensor surface, while inlets farther away have a reduced effect. In the most extreme case, shown by red streamlines, fluid enters and exits the reservoir, bypassing the sensor. To address this, each sampling inlet should be connected to the reservoir by a microchannel that enters opposite the outlet. These routing channels should be kept as short as possible and have minimal internal volume to reduce reservoir fill time. As demonstrated in the Martín *et al.* (2017) device, this can be achieved by shortening the channel lengths, which is most effectively done by clustering the inlets near each other and close to the reservoir.[47] However, the sampling inlets must remain sufficiently spaced to leave enough adhesive area between them for secure attachment to the skin, which is critical for maintaining structural integrity and preventing detachment or leakage during use.

Microchannels typically have a rectangular cross-section with width 'w' and height 'h', as shown in Fig. 3b. These dimensions are determined by the chosen fabrication method and flow dynamics. To minimize the volume of these connecting channels, their lengths should be reduced through inlet clustering, and their cross-sectional area should be kept as small as manufacturing constraints allow. However, reducing the channel size is limited by both fabrication resolution and the fluid forces involved. For instance, when channels are made from hydrophobic materials, a reduction in cross-sectional area increases the capillary backpressure, the pressure opposing fluid flow. If this backpressure exceeds the driving pressure generated by the sweat glands, flow can be completely obstructed. In the next section, we will show how to calculate both the capillary backpressure and the pressure drop due to viscous forces for the device shown in Fig. 3a. A detailed discussion of how pressure varies with channel geometry, along with its impact on sweat evaporation and the device's mechanical stability, is available in Koh *et al.*[28]

Besides basic microfluid designs, researchers can exploit biofluid properties and microfluidic effects to achieve precise fluid control, an essential requirement for wearable applications, by implementing channel actuators. For instance, capillary backpressure is the underlying principle of capillary bursting valves (CBVs), which are widely used as passive flow regulators. Choi *et al.* (2017) demonstrated this concept in a sweat collection and storage patch consisting of a network of interconnected reservoirs. In their design, CBVs directed sweat sequentially into each chamber, enabling time-resolved analysis of sweat composition.[48] The authors also provided a detailed discussion of the governing principles, fabrication workflow, and device characterization.

More recently, Ye *et al.* (2024) extended this concept to an aptamer-based biosensor for continuous oestradiol monitoring in sweat, where CBVs enabled autonomous and uninterrupted fluid routing.[49] Once the reservoir was filled, the excess fluid was redirected into an adjacent channel, providing the incubation time required for the biochemical reaction. This advancement highlights the versatility of passive valve systems for achieving both temporal and functional control in wearable biosensing applications.

Other forms of passive regulation include capillary pressure control valves (CPCVs), which operate at threshold pressures defined strictly by geometry and biofluid properties. Wang *et al.* (2021) provide a detailed account of the principles and applications of CPCVs, underscoring their potential for low-power, geometry-driven flow control.[50]

Beyond these fundamental examples, microfluidic flow control encompasses a wide variety of strategies. Passive systems rely on intrinsic physical forces, such as capillarity, wettability, or surface tension, shaped by device architecture. By contrast, active control methods deliberately perturb flow using external fields, pumps, or actuation forces, enabling dynamic control at the cost of added complexity. Gharib *et al.* (2022) provide an overview of these active strategies, which expand the design space for advanced wearable biosensors.[51] Readers interested in a deeper exploration of both passive and active flow regulation can refer to recent comprehensive reviews.[52–54]

Together, these examples illustrate how diverse microfluidic control strategies, from simple CBVs to complex active actuation, can be tailored to wearable biosensing applications. Passive designs excel in simplicity, scalability, and power-free operation, whereas active systems open the door to more adaptive and programmable control of biofluid sampling in real time.

The considerations outlined above are useful for conceptual design, where the system's overall configuration and functional elements are defined. They can also be used in the preliminary design stage, where critical dimensions, materials, and flow characteristics are specified and evaluated. Ultimately, the final design must be refined through iterative optimization, which may include adjusting the sensor geometry to meet performance requirements, incorporating more advanced manufacturing techniques, or relaxing design tolerances to reduce costs. Additional features such as Tesla valves, capillary valves, or integrated flow sensors may also be necessary to meet specific performance goals. The reader can find further information on advanced microfluidic theory in Bruus (2011),[39] and the applied approach can be found in Nguyen and Wereley (2006).[36] An example of how to apply the principles described in this section is provided in the case study below.

Case study: designing a wearable microfluidic biosensor for continuous lactate and sodium monitoring

Here we present a case study to illustrate how to systematically apply microfluidic design principles to develop a wearable biosensor. The proposed design is based on the theoretical concepts presented throughout the review and outlines a skin-mounted device for continuous monitoring of lactate and sodium in sweat during exercise. These analytes provide insights into muscle fatigue and hydration, making them valuable for athletic and health monitoring applications. The following discussion provides a comprehensive guide to integrating physiological constraints, fluid dynamics, and sensor requirements.

The design process begins by defining the system requirements and constraints (Fig. 1b). In this example, the primary requirement is to create a device that can be mounted on the skin and continuously monitor analyte concentrations during exercise. Although this case study focuses on sweat, the same design framework can be applied to other biofluids, such as saliva, tears, or interstitial fluid, by substituting the biofluid properties (*e.g.*, viscosity, density, surface tension) and operational conditions (secretion rate) into the analysis. By using the relevant parameters in the governing equations or in the supplemental code we provide (see code availability section), researchers can rapidly approximate flow regimes and identify design constraints specific to their device application.

Additional design requirements include the use of biocompatible materials, user safety, and comfort. Note that these criteria may vary depending on the specific application. Moreover, it is important to identify constraints that may include limitations related to budget, available equipment, development timeline, and manufacturing capabilities.

For this case study, we establish the requirement that the device should start measurements within twelve minutes of the onset of sweating (based on the time to fill the reservoir with an area that accommodates both lactate and sodium sensors). Next, a comparative and parametric analysis is performed. This involves reviewing existing devices and designs that meet, either fully or partially, the identified requirements. From these examples, key design parameters can be extracted, such as the target biofluid, material choices, and basic geometric configurations, as summarized in Table 2. This analysis serves not only as a reference point for establishing physiological and engineering limits but also as a guide for identifying opportunities to improve performance. Furthermore, it helps position the new design within the current landscape of wearable biosensors, ensuring it offers competitive advantages.

From the parametric study, we selected sweat as the target biofluid and an electrochemical sensor with the geometry shown in Fig. 3(a). The sensor has the following dimensions: width w_r = 3 mm, length ℓ_r = 12 mm, which results in a reservoir area $A_\mathrm{reservoir}$ = 36 mm^2.

The reservoir height h depends on the chosen manufacturing method and material. Table 5, "comparison of the different fabrication methods for wearable microfluidic systems", presents resolution ranges for several techniques. Based on this information, a reservoir height of h = 300 μm was selected. This value offers manufacturing flexibility, as many fabrication methods can achieve this resolution, and it aligns with budget and performance considerations identified in the parametric study. Thus, the resulting reservoir volume is:

$$V_\mathrm{reservoir} = A_\mathrm{reservoir} \times h = 36\ \mathrm{mm}^2 \times \left(\frac{300}{1000}\right)\mathrm{mm} = 10.8\ \mu\mathrm{L}$$

To meet the design requirement that sensing starts within 12 minutes of sweat onset, the device must collect and deliver enough sweat to fill the reservoir within that timeframe. Sweat is first collected through the sampling inlet, then routed through microchannels to the reservoir. A critical physiological constraint is the passive eccrine sweat secretion rate ν_sweat, which varies by individual and environmental conditions. Reported sweat rates range from 0.3 to 2.0 μL min^{-1} cm^{-2} under moderate activity, with 0.5 μL min^{-1} cm^{-2} commonly cited as a median value. During intense exercise, localized rates can reach 3–5 μL min^{-1} cm^{-2}, particularly in regions such as the forehead or upper back.[13,28,55]

Since ν_sweat is defined as volumetric flow rate per unit area, its units correspond to a velocity (*e.g.*, μm min^{-1}). This has direct implications for how quickly different components of the system will fill. For instance, the time required to fill a sampling inlet with cross-sectional height h_SI and area A_SI is given by:

$$t_\mathrm{fill,SI} = \frac{h_\mathrm{SI}}{\nu_\mathrm{sweat}}$$

This relationship shows that the fill time is dependent on the inlet height and the sweat secretion rate, not on the inlet area. To reduce $t_\mathrm{fill,SI}$, one can either increase ν_sweat through active methods such as iontophoresis for the delivery of cholinergic drugs (sweat stimulants), use of sweat creams, or decrease the adhesive layer thickness, which defines h_SI.

In this example, we assume an adhesive thickness of 50 μm and use the median sweat secretion rate of 0.5 μL min^{-1}

cm^{-2} (equivalent to 5 μm min^{-1}). The resulting filling time for the sampling inlet is:

$$t_{\text{fill,SI}} = \frac{h_{\text{SI}}}{v_{\text{sweat}}} = \frac{50\ \mu\text{m}}{5\ \mu\text{m}\ \text{min}^{-1}} = 10\ \text{min}$$

Since the total allowable time is 12 minutes, only 2 minutes remain to fill the reservoir, neglecting the inlet microchannel volume for this initial estimate. Thus, the required minimum flow rate is:

$$q = \frac{V_{\text{reservoir}}}{\Delta t} = \frac{10.8\ \mu\text{L}}{2\ \text{min}} = 5.4\ \mu\text{L min}^{-1}$$

We can now calculate the minimum sampling inlet area required to deliver the flow rate established earlier:

$$A_{\text{SI}} = \frac{q}{v_{\text{sweat}}} = \frac{5.4\ \mu\text{L min}^{-1}}{0.5\ \mu\text{L min}^{-1}\,\text{cm}^{-2}} = 10.8\ \text{cm}^2$$

This area is equivalent to a circular inlet with a diameter of approximately 37 mm. At this size, a single sampling inlet may be sufficient, and multiple inlets are likely unnecessary. Placing the sampling inlet close to the reservoir, as shown in Fig. 3a, minimizes the length of the channel between the MI and the reservoir. In this configuration, the channel volume is negligible, and we can estimate the total fluid volume in the system as the sum of the sampling inlet and reservoir volumes, yielding:

$$V_{\text{total}} = 53.2\ \mu\text{L (SI)} + 10.8\ \mu\text{L (reservoir)} = 64\ \mu\text{L}$$

Using this inlet area, the reservoir is replenished every two minutes. Although increasing the inlet area could further improve the refresh rate and temporal resolution, the system remains constrained by the sampling inlet filling time, previously calculated as 10 minutes. This sets a practical limit on how quickly the device can begin measurements. Reducing the reservoir volume, when possible, is an effective approach to improve temporal resolution and minimize dead volume.

To check the preliminary design, it is useful to compare it with previously published devices. The reservoir volume and estimated filling time are in line with the designs of Koh *et al.*,[28] which use 5–10 μL reservoirs that fill over approximately 0.3 to 3.2 hours depending on sweat rate (1.2–12 μL per hour), and of Martín *et al.*,[47] which employ an 8.24 μL reservoir requiring approximately 13.4 minutes to fill at a sweat rate of 0.66 μL min^{-1}. These comparisons support the feasibility of the preliminary design; however, further optimization should follow.

Before optimization, it is important to validate the initial design assumptions, namely that the flow is laminar, capillary forces are dominant, gravity is negligible, and convection is the primary mode of transport. These conditions can be evaluated using dimensionless numbers, as summarized in Table 1. The Reynolds number (Re) quantifies the balance between inertial and viscous forces. The Capillary number (Ca) compares viscous to surface tension forces. The Bond number (Bo) expresses the ratio of gravitational to surface tension forces and is used to confirm that gravity can be neglected. Finally, the Péclet number (Pe) determines whether convective transport dominates over molecular diffusion. The characteristic speed for these calculations is the average flow velocity (V_{avg}), and the characteristic length is the hydraulic diameter (D_{h}). Using the reservoir dimensions (w_{r} = 3 mm and h = 300 μm), the hydraulic diameter is:

$$D_{\text{h}} = \frac{4A}{P} = \frac{4 \times w_{\text{r}} \times h}{2(w_{\text{r}} + h)} = 2 \times \frac{3\ \text{mm} \times 3\ \text{mm}}{3\ \text{mm} + 3\ \text{mm}} = 0.55\ \text{mm}$$

where A is the cross-sectional area and P is the wetted perimeter.

And the average velocity can be calculated as:

$$V_{\text{avg}} = \frac{q}{w_{\text{r}} \times h} = \frac{5.4\ \mu\text{L min}^{-1}}{3\ \text{mm} \times 0.3\ \text{mm}} = 6\ \text{mm min}^{-1}$$

Using the physical properties of sweat (ρ = 1002 kg m^{-3}, μ = 1.01 mPa, σ = 38.5 mN m^{-1}), it is possible to calculate the dimensionless number values for the proposed system:

$$\text{Re} = \frac{\rho V D_{\text{h}}}{\mu} = \frac{1002\ \text{kg m}^{-3} \times \left(\frac{6\ \text{mm min}^{-1}}{60 \times 1000}\right) \times \left(\frac{0.55\ \text{mm}}{1000}\right)}{1.01 \times 10^{-3}\ \text{Pa s}} = 5.4 \times 10^{-2}$$

$$\text{Ca} = \frac{\mu V}{\sigma} = \frac{1.01 \times 10^{-3}\ \text{Pa s} \times \left(\frac{6\ \text{mm min}^{-1}}{60 \times 1000}\right)}{38.5 \times 10^{-3}\ \text{N m}^{-1}} = 2.6 \times 10^{-6}$$

$$\text{Bo} = \frac{\rho g L^2}{\sigma} = \frac{1002\ \text{kg m}^{-2} \times 9.81\ \ \text{m s}^{-2} \times \left(\frac{0.55\ \text{mm}}{1000}\right)^2}{38.5 \times 10^{-3}\ \text{N m}^{-1}} = 7.7 \times 10^{-2}$$

$$\text{Pe} = \frac{VL}{D} = \frac{\left(\frac{6\ \text{mm min}^{-1}}{60 \times 1000}\right) \times \left(\frac{0.55\ \text{mm}}{1000}\right)}{1.0 \times 10^{-9}\ \ \text{m}^2\ \text{s}^{-1}} = 55$$

Diffusion coefficient of a small molecule $D \approx 1.0 \times 10^{-9}$.[4]

Both the Reynolds number and the Capillary number are much less than 1, confirming that the flow is laminar and that viscous and capillary forces govern the dynamics. The Bond number is also well below 1, indicating that gravitational effects are negligible compared to surface tension. Furthermore, the Péclet number is significantly greater than 1, showing that convective transport dominates over diffusion. Together, these results support the use of simplified flow models and validate the assumptions made during the early design stages.

Since Re ≪ 1 the flow is laminar. Similarly, because Ca ≪ 1 capillary forces are dominant, but they dominate only during the initial filling phase when the fluid encounters a free (dry) surface. Once the reservoir is wetted and a steady outflow is established, no free surface remains, and viscous forces become dominant. The small Bond number confirms that gravity can be neglected, while the relatively large Péclet number indicates that convection governs solute transport along the flow path. For simplicity, we begin by analysing the steady state, where viscous and convective effects dominate, and later address the initial dry state, where capillary effects are most significant.

In our system, flow is driven passively by the secretory pressure of eccrine sweat glands, which typically produce pressures in the range of 1.3–2.5 kPa during activity. However, a conservative upper limit of ~10 kPa is often assumed in design contexts based on estimates from select experimental studies.[62,63] Therefore, the total pressure drop must remain below this threshold to enable sweat flow through the device. The viscous pressure drop (resistive flow) has an exact analytical solution for laminar flow.[39] However, we employ an approximation within 10% of the exact solution, which is particularly useful for highlighting the interplay among channel length, flow rate, and channel width and height. This simplification allows us to evaluate how geometric parameters and operating conditions together determine the feasibility of sweat transport through the device, while the accompanying Colab notebook provides the exact solution for comparison

$$\Delta P = \frac{12\mu LQ}{wh^3\left(1 - 0.63\dfrac{h}{w}\right)} = 0.17\ \text{Pa}$$

We also consider the pressure drop in the outlet channel, assuming a width of 100 μm to reduce sweat evaporation[28] and a length of 1 mm:

$$\Delta P = \frac{12\mu LQ}{wh^3\left(1 - 0.63\dfrac{h}{w}\right)} = 4.6\ \text{Pa}$$

The viscous pressure drop (4.77 Pa) is substantially smaller than the 10 kPa available from sweat glands, indicating sustainable flow after filling. We now evaluate capillary pressure, which dominates initial filling. The capillary pressure is given by the Young–Laplace equation:

$$\Delta P = 2\sigma\cos(\theta)\left(\frac{1}{w} + \frac{1}{h}\right)$$

where σ is the surface tension and θ is the contact angle. For hydrophilic materials ($\theta < 90°$), $\Delta\text{Pc} > 0$ (driving flow). For hydrophobic materials ($\theta > 90°$), $\Delta\text{Pc} < 0$ (opposing flow). We analyze the critical case of PDMS ($\theta \approx 110°$; see Materials section for more details):

$$\Delta P = 2 \times 0.0385\frac{N}{m}\cos(110)\left(\frac{1000}{3\ \text{mm}} + \frac{1000}{0.3\ \text{mm}}\right) = -97\ \text{Pa}$$

Although PDMS is used here as a representative example due to its widespread use in wearable microfluidics, the same design principles apply to other elastomers and coatings; the key parameter that changes is the contact angle, which directly determines capillary forces. It is important to keep in mind that we provided a supplemental code where readers can input material-specific wettability values to recalculate the relevant flow parameters.

For the current design, the worst-case pressure drop (viscous + capillary) is approximately 100 Pa. This value is well below the 10 kPa physiological limit, confirming that sweat can flow passively through the microchannel without assistance. If the pressure drop exceeded 10 kPa, sweat glands could not overcome the hydraulic resistance, and flow would cease. A pressure drop equal to 10 kPa would permit flow only under ideal conditions, resulting in unreliable performance. Therefore, maintaining a pressure drop significantly below this limit, as demonstrated here, ensures reliable operation across different physiological conditions.

To summarize, this case study illustrates the design of a wearable microfluidic device for lactate and sodium monitoring in sweat, consisting of a 10.8 μL reservoir (3 mm width, 12 mm length, 300 μm height) fed by a 37 mm sampling inlet. The system operates under passive sweat secretion pressures (≤10 kPa) with a total pressure drop of <100 Pa, ensuring stable continuous flow. Dimensionless analysis confirms laminar flow dominated by viscous and capillary forces ($\text{Re} \ll 1$, $\text{Ca} \ll 1$), negligible gravitational influence ($\text{Bo} \ll 1$), and convection prevailing over diffusion ($\text{Pe} \gg 1$). With an inlet filling time of 10 min and a reservoir refreshing rate of 2 min, the design meets the requirement of starting measurements within 12 min of sweat onset. Fig. 4 illustrates the parameters generated using our Jupyter Notebook for this same case study.

This case study outlines a method for developing a preliminary design that satisfies the defined requirements and constraints. It is important to note that the parameters are calculated under an idealized case. In practice, wearable devices may experience transient flow variations, air bubble formation, or motion-induced pressure fluctuations. To mitigate these effects, researchers often incorporate redundancy in inlet placement, apply hydrophilic surface treatments, add mechanical support layers to stabilize channel geometry during use, and use auxiliary sensors such as flow rate, moisture, and accelerometers so signal processing can be performed to filter background noise. The wearable microfluidic device may need to undergo several iterations through the design process until all critical requirements are met or, if necessary, relax certain constraints based on feasibility. Once refined, a prototype can be fabricated for experimental testing and validation under the expected operational conditions identified during the parametric study.

During testing, special attention must be given to key performance metrics. Sensors must remain wet, adhesive seals must withstand mechanical strain, and the flow behaviour should match the expected laminar pattern. Specifically, entering from one side of the reservoir and exiting from the opposite side to continuously refresh the

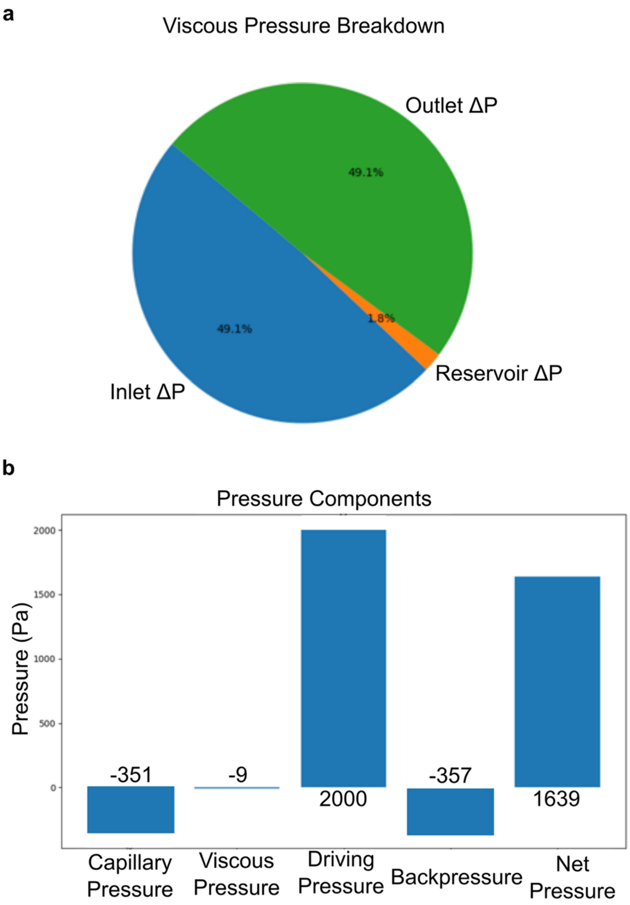

Fig. 4 a) Viscous pressure drop within the channel network. This plot represents the pressure losses in the flow due to viscous forces. The larger viscous pressure drops occur in the microfluidic inlet (MI) and in the outlet channels. b) Pressure distribution in the microfluidic system. This plot shows the pressures acting on the microfluid device due to the viscous forces, capillary forces, and the natural driving pressure from the sweat glands. The backpressure is the result of the addition of the viscous pressure and capillary pressure, while the net pressure is the result of the addition of the driving pressure (positive pressure) and backpressure (negative pressure). The resulting net pressure should be positive to have a continuous forward flow.

fluid. This behavior can be assessed in bench-top tests using a syringe pump and dyes for flow visualization before on-body testing.

To aid in the design and prototyping stages, a companion Colab notebook has been provided with this tutorial review to operationalize the review's design workflow into interactive, reproducible calculations for early-stage microfluidic systems. Users can specify a few intuitive inputs, such as material and biofluid (or custom ρ, μ, σ, θ), reservoir geometry and height, inlet/outlet channel widths and lengths. The code then computes core geometric quantities (areas, volumes, hydraulic diameter), estimates capillary pressure *via* Young–Laplace equation, evaluates viscous pressure losses with rectangular-duct models, and reports key dimensionless groups (Re, Ca, Bo, We) to validate laminar, capillarity-relevant conditions.

Additionally, the code budgets inlet wetting and reservoir fill times from secretion rate and footprint, then assembles a net pressure margin to quickly flag PASS/FAIL feasibility for passive flow. Lastly, the outputs are presented as labelled tables and clear top-view schematics with dimension lines. To ensure reliability, defaults and safeguards are built in to make the widgets robust, and all units are explicitly handled to minimize errors. Taken together, the notebook transforms the equations presented in this review into a design aid that enables readers to iterate rapidly toward viable channel and reservoir designs.

Even though the supplemental code can streamline the early-stage design, several issues may arise during prototyping. Air bubbles can become trapped inside the reservoir, blocking fluid flow to the sensor. This often occurs when a hydrophobic sensor is surrounded by hydrophilic surfaces, which may require surface treatments or a change in materials. Sampling inlets may fail to collect sweat effectively, suggesting they are either too small or not aligned with active sweat glands. Significant deformation or collapse of the channels and reservoir may indicate the need for stronger or more stable materials. Fluid leakage can also occur, often due to an inadequate adhesive layer or other flaws in the manufacturing process that must be addressed. Design iteration is often necessary to resolve these issues. The following sections provide a deeper analysis of fabrication methods, material selection, and system optimization.

Design requirements and constraints for wearable microfluidics

Design requirements

Although several materials and methods are available for fabricating microfluidic devices, they must meet certain key requirements to ensure reliable sensing performance in a wearable format. These include maintaining continuous flow, minimizing sample contamination, and reducing the time between sample collection and analyte detection. This section discusses each of these requirements and the strategies used to optimize the performance of the microfluidic system.

The primary goal of wearable biosensors is to monitor real-time changes in analyte levels in a non-invasive and continuous way. In addition to using flexible materials to ensure mechanical compliance with skin and body movements,[64] a key design consideration is how to move biofluids through a microfluidic system without relying on bulky external equipment. To address this, wearable biosensors can use either passive or active fluid transport methods.[65]

Epidermal sweat microfluidics rely on the pressure generated by sweat glands to drive flow. However, incorporating additional transport mechanisms can enhance biofluid movement within a system. Passive methods, such as capillary action, osmosis, or surface tension, are generally simpler and more cost-effective. For example, Sempionatto *et al.* improved tear flow control by employing a hydrophilic polycarbonate membrane to draw tears from the eye and a paper outlet to wick fluid through the system.[66] Zhang *et al.* took a different approach by applying surface modifications to create gradients in surface tension to drive sweat flow.[67] Active methods, on the other hand, offer greater control over the biofluid flow. Lin *et al.* demonstrated this by incorporating an array of thermo-responsive, micro-heater-controlled hydrogel valves that actively regulate fluid collection, routing, and compartmentalization.[65] When heated above their lower critical solution temperature (LCST), the hydrogels shrink to open the channels and permit flow; when cooled, they re-swell to block the channels.

Wearable biosensors must also optimize the interaction between the target analyte and the biorecognition element, commonly known as the incubation time. This interaction is highly dependent on the speed at which the biofluid moves through the system. If the fluid flows too quickly, the analyte may not have enough time to bind to the sensing surface, reducing detection efficiency. On the other hand, lower flow rates can lead to analyte accumulation, potentially saturating the signal. To address this, Cheng *et al.* patterned hydrophilic and hydrophobic regions within microfluidic channels to modulate flow rate and enhance signal reliability.[68] More hydrophobic regions were incorporated in areas, such as the lactate and magnesium sensing zones, where slower movement was needed to ensure optimal reaction times between analytes and the sensing surface. Similarly, Nightingale *et al.* incorporated a miniature pumping system to precisely control the interaction time between analytes and reagents before detection.[69]

Beyond fluid control, incubation time can also be molecularly and electrically tuned. For instance, a duo strategy was demonstrated by Ye *et al.* when combining the CBV to stop and redirect the flow, with the use of aptamers, a single-stranded DNA sequence, to detect hormones in

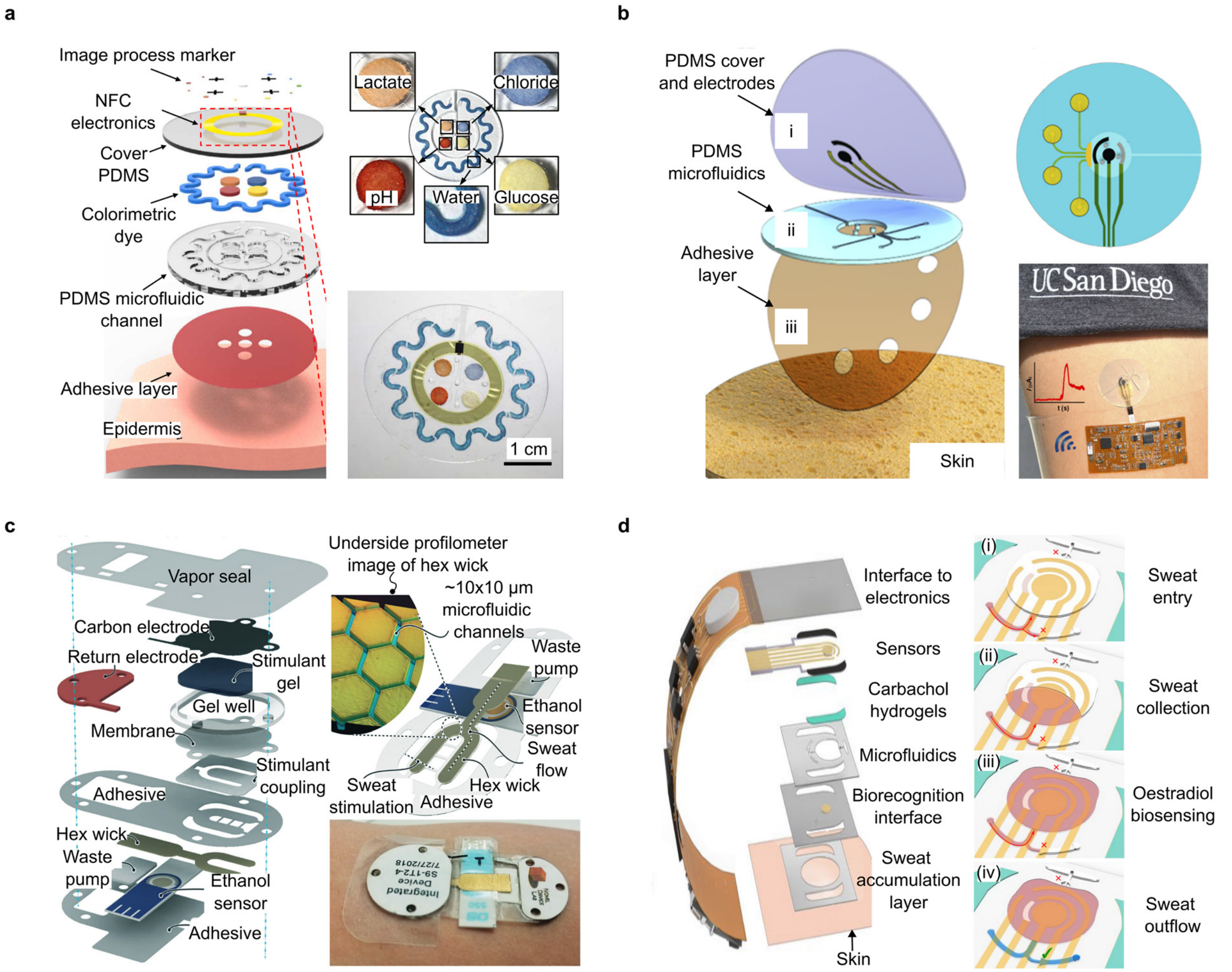

Fig. 5 Polymer-based microfluidic wearable biosensors. a) Integration of PDMS-based microfluidics with paper-based colorimetric detection of several metabolites and pH in sweat.[28] b) PDMS electrochemical sensor for measurement of glucose and lactate in sweat. Fig. (i)–(iii) represent the layers creating the microfluidic channel and reservoir.[47] c) Sweat transport through gold-modified PET hexagonal wick for detection of ethanol in sweat.[71] d) PET-based microfluidic channels and valves for oestradiol detection in sweat. Fig. (i)–(iv) represent the microfluidic and biosensor workflow.[49] [a) This figure has been adapted from ref (28) with permission from The American Association for the Advancement of Science, Copyright 2016; b) This figure has been adapted from ref (47) with permission from American Chemical Society, Copyright 2017; c) This figure has been adapted from ref. (71) with permission from the Royal Society of Chemistry, Copyright 2018; d) This figure has been adapted from ref. (49) with permission from Springer Nature, Copyright 2023].

sweat. The CBV ensured enough time for the immune reaction (Fig. 5d), and they showed that applying a voltage to the electrochemical system could accelerate the reaction between the analyte and the aptamer,[49] for further discussion on the use of aptamers in wearable biosensing see also Mayol *et al.*[70] Overall, microfluidic systems should incorporate strategies that support appropriate incubation times, ensuring effective signal generation.

Decreasing time lag is directly related to real-time monitoring. Temporal resolution is another critical factor in wearable biosensors. To enable real-time monitoring, the time between sample collection and analyte detection must be minimized. One strategy is to accelerate the sample collection process. For example, Nyein *et al.* introduced a hydrophilic hydrogel to reduce dead volume within the microfluidic system and channel sweat as soon as it is secreted.[61] Similarly, the use of low volume of sweat ensures minimal dead volume as demonstrated by Hauke *et al.* and their "hex-wick" microchannel material to speed sweat collection from the skin (Fig. 5c).[71]

Another key requirement of wearable biosensors is maintaining sample purity. Contamination can arise from various sources, including body creams, skin oils, and dead cells. For epidermal wearables, keeping the skin surface free of such contaminants is one of the most important requirements. Peng *et al.* addressed this by introducing a combined oil layer and sweat-permeable membrane that reduces the entry of skin contaminants into the sensor.[72] Another source of contamination is sample carryover (accumulation) from previously collected fluids. Nyein *et al.* tackled this by designing a sweat reservoir that measures analytes from freshly collected sweat and releases older sweat into a separate microfluidic channel.[73] In addition to separating fresh and old samples, material modifications can also be used to prevent contamination due to analyte adhesion on microfluidic surfaces.[64,74]

Design constraints

Although all microfluidic devices must meet the functional requirements discussed above, they must also operate within specific physiological and physical constraints. These constraints are largely imposed by analyte dynamics in the body, biofluid behavior, and fluid properties, which are discussed in this section.

Wearable sensors use non-invasive biofluids to indirectly measure changing analyte levels in blood. To achieve this, several steps must occur, each introducing a time lag between changes in blood and detection by the sensor. First, analytes must partition through biological barriers to reach the target biofluid. For example, analytes need to diffuse from blood vessels to sweat glands for sweat-based sensing.[75] Next, a sufficient volume of biofluid must accumulate in the sensing area for reliable detection. Finally, the analyte and biorecognition element need to incubate to generate a measurable signal. Together, these steps introduce a time delay that must be considered in the design of wearable sensors. Bolat *et al.* explored these challenges in their study on an integrated sweat stimulation, collection, and analysis platform. The authors showed that variability in the time it takes to fill the sensing reservoir limited real-time glucose monitoring in diabetic patients.[76]

In addition to analyte behavior, biofluids present variable parameters such as flow rate, secretion volume, and evaporation rate. Each of these affects how frequently fresh biofluid can replenish the sensing area, a factor known as refresh rate. This, in turn, impacts the temporal resolution between analyte levels in non-invasive biofluids and their fluctuations in blood. Moreover, biofluid parameters vary depending on the secretion mechanism, collection method, individual physiology, and environmental conditions. For example, sweat induced by a cholinergic agonist typically flows faster and in greater volume than passive sweat, and individual responses to the drug may vary, causing fluctuations in sweat production.[61] Environmental factors like temperature and humidity further affect the rate and volume of secretion, as well as how quickly the fluid evaporates. These variations must be considered during sensor design to ensure consistent performance.

Finally, the physical properties of the biofluid, such as viscosity, density, and whether it behaves as a Newtonian fluid (whether its viscosity is constant under different conditions of shear stress), influence how the fluid moves through the microfluidic channels. These characteristics must be accounted for during the system design phase. Table 3 compares the different biofluid parameters that researchers must consider when developing a wearable system. For instance, sweat has low viscosity and density, similar to water, and flows easily through most microfluidic systems.[77] In contrast, interstitial fluid is more viscous and may move more slowly unless the system is designed to accommodate its properties.[78] Furthermore, when evaluating microfluidic performance on the bench, it is important to test with fluids that closely mimic the target biofluid to accurately model flow behavior.

Fabrication principles of microfluidics for wearable sensors

The successful integration of microfluidics into wearable platforms relies on the careful selection of materials, fluid collection mechanisms, and fabrication methods. Wearable systems must have similar mechanical properties to the skin to ensure conformal contact with the body and reliable operation.[64] This introduces unique challenges for fabrication and material selection since microchannels need to preserve both stretchability and structural integrity under mechanical deformation.[28]

In wearable and implantable technologies, microfluidic systems are necessary because they allow for the control and manipulation of small volumes of body fluids.[13] Furthermore, microchannels are key elements in minimizing

Table 3 Comparison of the physical properties of different biofluids

Biofluid	Density (kg m^{-3})	Viscosity (mPa s)	Surface tension (mN m^{-1})	Newtonian behavior	Ref.
Sweat	1002	1.01	72	Newtonian	76, 77, 79
ISF	1000	3.5	—	Newtonian	77, 78
Tears	1000	4.4–8.3	42–46	Non-Newtonian	78, 80, 81
Saliva	1002–1012	2.63	57.7	Non-Newtonian	82–85
Water[a]	997	0.912	72.8	Newtonian	—

[a] Values at ambient temperature (20–25 °C).

sample leakage, evaporation, and contamination.[86] Careful design and engineering are reflected in choosing the system's material, composition, and geometry.

This section provides an overview of the key elements for the successful fabrication of microfluidics for wearable applications. We first review commonly used materials (polymers and paper-based systems), highlighting their advantages, limitations, and use cases. We then describe fabrication techniques with an emphasis on simplicity, reproducibility, and scalability.

Materials

Polymers. Polymers are large molecules made of repeating monomer units. Based on their response to heat, they can be classified as thermoset (at high temperatures they decompose without melting), thermoplastic (at high temperatures they soften), and elastomers (they can change their shape under external forces and return to their original state after removal).[87] Polymers are typically used for the fabrication of microfluidics due to cost-effectiveness, biocompatibility, optical transparency, and mechanical properties similar to those of the skin (low Young's modulus and elasticity).[13]

PDMS is the most used material for microfluidics fabrication due to its low cost and mature manufacturing methods.[12] PDMS is an elastomer with ideal properties for microchannel fabrication. Its Young's modulus (360 kPa to 870 kPa) compares to that of the skin's forearm (20 kPa to 850 kPa). Note that skin's mechanical properties depend on several factors, such as age.[88] Moreover, PDMS's low curing temperature, chemical inertness, thermal stability, optical transparency, ability to conform to different surfaces, and release from them without damage make it one of the most used materials for microfluidics in wearable and biological devices.[21,74]

PDMS can be acquired through commercially available kits; the most common being the Sylgard R 184 from Dow Corning Corporation.[89] These kits usually have two solutions consisting of the monomer and the curing agent. The solutions are combined in a 10 : 1 weight ratio. However, this ratio can be tuned to achieve the desired mechanical and optical properties.[74] For instance, to obtain flexible PDMS with a Young's modulus similar to the skin, a 30 : 1 base/curing-agent ratio can be used.[47] Furthermore, PDMS is compatible with several fabrication methods, such as soft lithography,[21] hot embossing,[89] and laser ablation replica molding,[90] among others, which will be discussed in the next section.

Due to its ease of use and mechanical properties, PDMS is the preferred polymer for creating microfluidics for wearable applications. One of the most representative examples of using PDMS for wearable microfluidics is from the work in the Rogers group. They pioneered a wearable microfluidic system for colorimetric sensing of ions, glucose, and lactate in sweat (Fig. 5a).[28] The device consisted of an adhesive layer for contact with the skin, a PDMS layer with the patterned microchannels, paper-based colorimetric sensors, and a cover PDMS layer, which embedded the near-field communication (NFC) electronics and antenna. The layers were fabricated through soft lithography and mechanical punching of the sweat collection inlets.

PDMS-based wearable microfluidic systems can be integrated with different detection techniques besides colorimetric sensing. Martín *et al.* developed a flexible microfluidic platform for continuous electrochemical measurement of glucose and lactate in sweat (Fig. 5b).[47] The system consisted of a top PDMS layer containing electrodes, a second PDMS layer that defines the microchannels, and a medical-grade adhesive tape containing the sample inlets in contact with the skin. The device was able to fill the detection reservoir after 8 minutes of exercise. For fabrication, the authors used soft lithography for mold creation and PDMS casting onto the mold to create the microchannels.

Despite its widespread use, working with PDMS for wearable microfluidics presents several notable limitations. Fabrication typically requires access to specialized facilities, such as a cleanroom, to achieve reproducible molds and fine features, or alternative soft lithography setups that can still be costly and time-consuming. Bonding PDMS layers often depends on oxygen plasma treatment to activate the surfaces for adhesion, which can introduce complexity in scaling up fabrication.

Because PDMS is a silicon-based elastomer with intrinsically low surface energy, adhesion of metals, inks, and other functional materials is poor, making stable electrode fabrication directly on its surface extremely challenging. Another limitation of PDMS is its hydrophobicity, which creates flow resistance in the microchannels, requiring external treatments or coatings to increase its hydrophilicity.[74] Furthermore, the hydrophobic nature of PDMS can lead to non-specific absorption of proteins in the microchannels, altering the local concentration of analytes and leading to biofouling and protein denaturation.[91] To address this issue, gas phase treatments with plasma, ozone, or UV light are used to tune PDMS hydrophilicity.[86] Plasma etching is the most common technique used to change the roughness and wetting properties of the microchannel surface to define hydrophobic and hydrophilic regions.[12] Piranha etching, chemical vapor deposition, and silanization are also alternatives for PDMS surface modification.[91]

Owing to its versatility and compatibility with different fabrication methods, it is possible to combine polymers with other materials and geometries to develop microfluidic devices. For instance, Hauke *et al.* designed a device that integrates sweat stimulation through iontophoresis, a PET-based gold-modified wick structure as inlets/microchannels, and an ethanol electrochemical sensor (Fig. 5c).[71] Their major contribution was the use of a polymer-based material with hexagonal-shaped microchannels as a wick (hex wick). Its function is to transport low volumes of sweat from the stimulation site to the sensors and the waste pump. The microchannels are formed by the gap between the hexagons. The fabricated inlet/microchannels were realized through a UV roll-to-roll process and sputtered with gold to eliminate analyte exchange.[92] The authors used the ethanol enzymatic sensor to validate the blood-to-sweat ethanol correlation and estimated lag times.

While PDMS (hydrophobic) is highlighted in the text as an illustrative material, the underlying fluidic principles remain valid across alternative substrates. The main effect of changing materials (hydrophilic) is a shift in wettability, reflected in the contact angle, which in turn alters capillary behavior. To account for this, we include supplemental code that allows readers to choose among a list of different substrates (PDMS, SEBS, PET, and glass) to explore design outcomes for a range of material choices.

Moreover, polymers can be used to fabricate flow control microfluidic elements such as valves and pumps. Ye *et al.* used polyethylene terephthalate (PET) to develop an autonomous microfluidic oestradiol sweat immunosensor (Fig. 5di).[49] Their microfluidic design included an inlet, outlet, sensing reservoir, and two CBVs. The CBV pair stops the flow inside the reservoir to ensure incubation time for the immunosensor in a steady state sample, without the influence of flow. Sweat would flow until the reservoir was filled. After that, the CBV would divert the remaining sweat flow to a second outlet. The flow follows the path of least resistance, which is typically through the larger channels (Fig. 5dii). The microfluidic layers consisted of double-sided adhesives and PET films patterned through a laser cutter. With this system, the authors showed a high blood-to-sweat oestradiol correlation during menstrual cycles.

Paper. The use of paper as a microfluidic substrate is convenient due to its low cost and lightweight properties, which make it ideal for portable devices.[13] Paper-based microfluidic devices are generally considered to be used for point-of-care and disposable systems. Their low cost and ease of fabrication make them ideal candidates for developing diagnostic systems for low-resource settings.[93] Paper can also be an ideal material for wearable devices due to its hydrophilic nature, ease of use, flexibility, and biocompatibility.[16]

Paper-based microfluidic devices exploit the capillary flow to move the fluids across the device without external forces. For precise flow control, cutting or chemical surface modification techniques are used to create hydrophilic and hydrophobic regions.[11,93] Furthermore, several types of paper (filter paper, nitrocellulose membranes, office paper, chromatography paper) can be combined to tune the properties of the proposed microfluidic system. Paper choice depends on capillary flow time, thickness, pore size, porosity, and surface quality, which will be dictated by the application requirements.[18]

Modification of the paper surface can be achieved by several methods. Ghosh *et al.* described a method for low-cost microchannel definition on paper-based microfluidics.[94] Their method relies on defining hydrophobic regions on the paper with toner ink deposited by laser printing. After deposition, the substrate is baked to melt the ink into the paper and define the microchannels (Fig. 6a). This technique allows for rapid fabrication and enables automation, thus minimizing human errors. Other techniques compatible with paper-based microfluidics include photolithography, wax printing, inkjet printing, plasma treatment, embossing, and origami-based shaping.[18]

Paper-based microfluidics are compatible with several sensing methods in wearable devices, enabling flexible integration of both optical and electrical transduction mechanisms. For instance, Mogera *et al.* developed a plasmonic sensor that uses surface-enhanced Raman spectroscopy (SERS) to measure sweat loss, sweat rate, and uric acid levels in sweat.[95] The system consists of a PDMS encapsulation layer, a chromatography paper microfluidic channel, plasmonic sensors, and a double-sided adhesive for contact with the skin (Fig. 6b). To obtain better measurements and stable SERS enhancement, the authors modified the chromatography paper with gold nanorods. Highlighting paper's versatility, Parrilla *et al.* developed a wearable chemiresistor for monitoring sweat rate and loss, using commercial filter paper coated with single-walled carbon nanotube ink.[96] In this case, the sensor relied on changes in electrical resistance caused by water absorption, demonstrating that paper can serve not only as a passive microfluidic conduit but also as an active sensing interface across multiple detection strategies.

Owing to its ease of use, paper can be combined with different materials for microfluidic channel creation. Sempionatto *et al.* developed a wearable biosensor for detecting alcohol, glucose, and vitamin concentrations in tears.[66] The system was placed on the nose bridge pad of a pair of eyeglasses to ensure non-invasive, continuous monitoring. Tears were stimulated and then collected through a microfluidic system for sensing (Fig. 6c). The

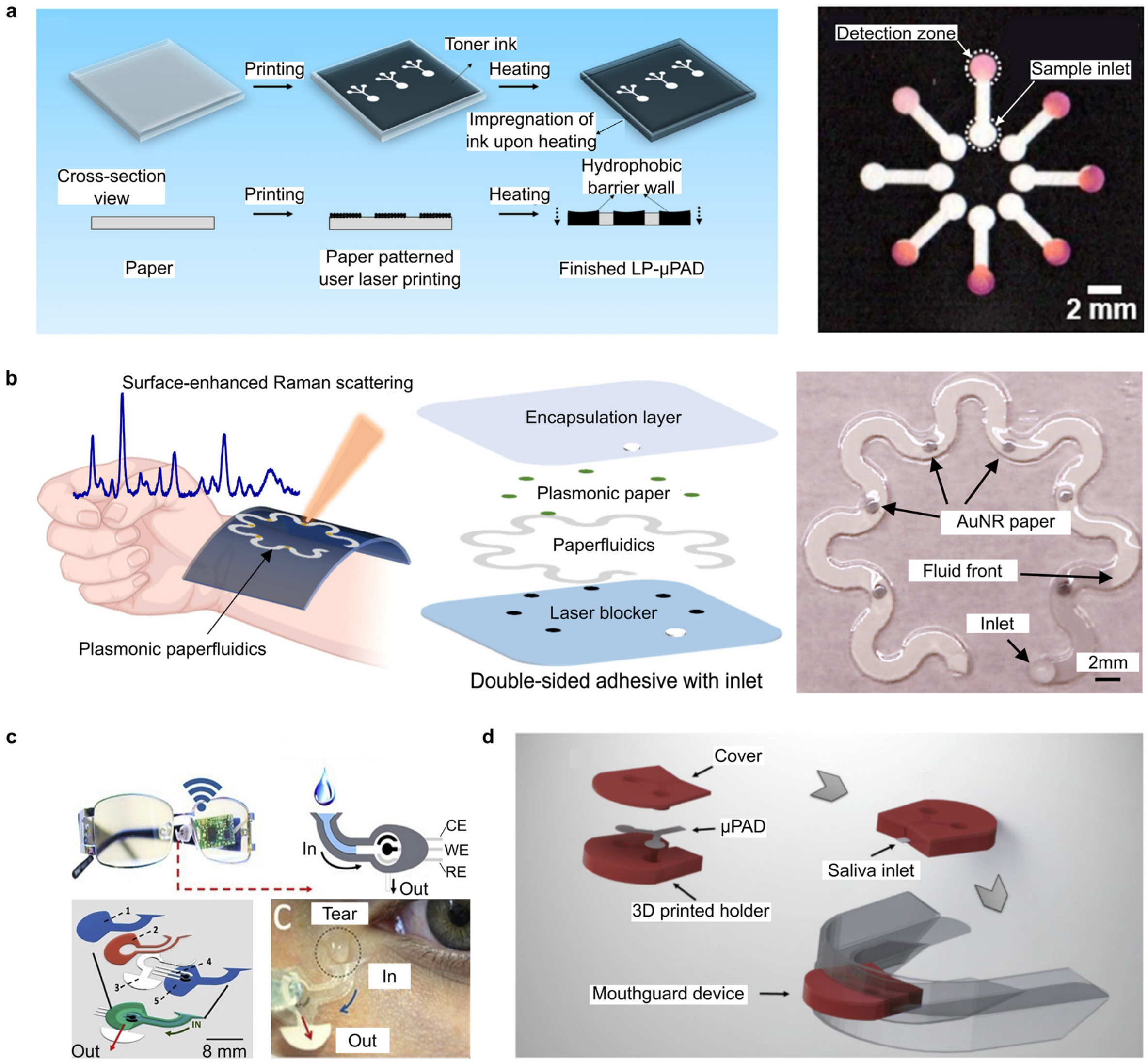

Fig. 6 Paper-based microfluidic wearable biosensors. a) Microchannel definition by deposition of toner ink over paper-based microfluidics.[18] b) Raman spectroscopy paper-based microfluidics for detection of sweat loss, sweat rate, and uric acid levels in sweat.[95] c) Paper-based wearable biosensor for detecting alcohol, glucose, and vitamin concentrations in tears.[66] d) Paper-based mouthguard biosensor for detecting glucose and nitrite concentrations in saliva.[97] [a) This figure has been adapted from ref. (18) with permission from Springer Nature, Copyright 2019; b) This figure has been adapted from ref. (95) with permission from The American Association for the Advancement of Science, Copyright 2022; c) This figure has been adapted from ref. (66) with permission from Elsevier, Copyright 2019; d) This figure has been adapted from ref. (97) with permission from Springer Nature, Copyright 2019].

microchannel used different layers comprising filter paper, polymers (PET, polycarbonate), and double-sided adhesives. The paper layer was used to define an outlet for the collected tears. It directed the tear flow outside the sensing reservoir, allowing tears to evaporate. The device was built as an alternative to a contact lens for non-invasive tear analysis outside the eyes. Contact lens-based biosensors can cause infection, irritability, and discomfort.

Besides tears, paper-based microfluidics can be used to monitor analytes in other biofluids such as saliva. De Castro *et al.* developed a paper-based microfluidic device (μPAD) for salivary diagnostics, capable of detecting glucose and nitrite as biomarkers for diabetes and periodontitis, respectively (Fig. 6d).[97] The paper-based microfluidic system included two detection zones, one for each analyte measured, and a sampling zone connected through microchannels. Moreover, the authors integrated the μPAD with a silicone mouthguard for wearable-format sensing of salivary biomarkers.

In summary, the selection of materials plays a pivotal role in the design and performance of wearable microfluidic devices (Table 4). Polymers like PDMS and SEBS (styrene–ethylene–butylene–styrene) offer flexibility and biocompatibility, making them ideal for skin-interfaced applications. Meanwhile, paper-based substrates provide a low-cost, lightweight alternative with inherent hydrophilicity and capillary action for passive fluid transport. However, it is important to notice that despite all the advantages offered by paper-based sensors, there are important limitations regarding the use of paper in a wearable device. Wearability introduces considerations such as skin conformability, mechanical robustness under motion, reusability, and seamless integration with sensors and electronics. These requirements define a design space that differs fundamentally from porous paper substrates and is more effectively addressed by polymeric engineered microchannels. By emphasizing these aspects, the review aims to guide readers toward practical design decisions that enable reliable, long-term, and multifunctional wearable biosensing platforms. As we transition into the next section on fabrication techniques, the choice of material will not only determine the functional performance of the microfluidic device but also the most suitable and scalable methods for its manufacturing.

Fabrication methods. The fabrication of microfluidics for wearable sensors is a critical step in translating proof-of-concept designs into functional devices. This process involves the integration of flexible materials to manufacture precise microchannel architectures. This section explores the primary methods used to fabricate microfluidic systems for wearable applications, including soft lithography, laser ablation, screen-printing, 3D printing, and large-scale techniques (Fig. 7).

Laminates. Laminate microfluidic devices are created by stacking independent layers cut by knife plotters, laser cutters, or other cutting tools, to form microfluidic devices (Fig. 7a).[102] The main advantage of this methodology is the compatibility with an extensive choice of layer materials. The combination of polymers, adhesives, and other substrates allows for tuning the mechanical and optical properties of the system.[87] Furthermore, they allow for rapid prototyping since bonding of the layers relies on techniques like simple adhesives or thermal bonding.[102]

Fabrication of microfluidic systems through laminates is one of the most popular techniques used in the design of wearable sensors. For instance, Wang *et al.* designed a wearable biosensor for monitoring essential amino acids and metabolites in sweat using a layered microfluid device.[100] The system combined two types of medical adhesives, PET and polyimide, to build the microfluidics and sensing chambers. The wearable patch consisted of four layers that were patterned and cut by a CO_2 laser, making the manufacturing scalable and low-cost. Moreover, the device integrated a sweat stimulation system composed of cathode/anode electrodes and hydrogels loaded with sweat-inducing drugs.

Laminate manufacturing enables fast fabrication and prototyping of microfluidics. One example that highlights this advantage is the "bear-like" wearable patch developed by Sun *et al.*, which can be manufactured in minutes.[101] The authors used a "cut and paste" fabrication method to pattern PDMS and PET films for the creation of the microchannels. Their method involved patterning all layers with a knife plotter, removing the excess material, and stacking each layer for assembly. The patch was able to detect glucose and lactate in sweat after chemical stimulation.

Laminate manufacturing also allows for the easy integration of electronics and antennas for wireless communication from the patch to an external receiver. Vertical integration of these elements reduces the wearable's footprint, increasing wearability and comfort. Liu *et al.* developed a wearable sensor for glucose and pH measurements in sweat.[98] The analytes were detected with colorimetric paper strips, and color intensity was measured using a smartphone. The microfluidic chip consisted of an adhesive layer to interface with the skin, a PDMS-based channel layer that serves as housing for the colorimetric strips, and a PDMS cover layer. To ensure proper flow and collection of sweat, the PDMS channels were coated with a surfactant (Triton X-100) to increase their hydrophilicity. Fabrication of the microchannels was done through soft lithography and plasma treatment to bond both PDMS layers.

Soft lithography. One of the most traditional fabrication techniques for microfluidics is soft lithography. Soft lithography creates master molds for microfluidic fabrication (Fig. 7b).[86] First proposed by the Whitesides group, the process begins by designing the microfluidic structures in a computer-aided design (CAD) program and printing the file on a transparent substrate for the photomask. The mold is created by etching a negative photoresist, usually SU-8, on a silicon wafer. Afterwards, a polymer (usually PDMS) is spread onto the master mold and cured before being peeled off.[21]

This method allows for high-resolution replica fabrication and stacking of a reduced number of layers for 3D geometry generation. However, care must be taken when removing the

Table 4 Comparison of the different materials for wearable microfluidic systems

Material		Key properties	Limitations	Ref.
Polymer	PDMS	Biocompatible, optically transparent, flexible, chemically inert, low Young's modulus	Its hydrophobic surface requires post-fabrication treatment	47, 98
	SEBS	Biocompatible, flexible, easily patterned	Less mature for microfluidics, often combined with other materials	99
	PET, polycarbonate, other thermoplastics	Mechanically robust, optically transparent, chemically inert	Rigid, needs precise bonding, less stretchable	100, 101
Cellulose-based material	Various types of filter paper (office paper, chromatography paper)	Low cost, lightweight, hydrophilic, flexible, porous	Variable quality, lower manufacturing resolution, susceptible to degradation	66, 95

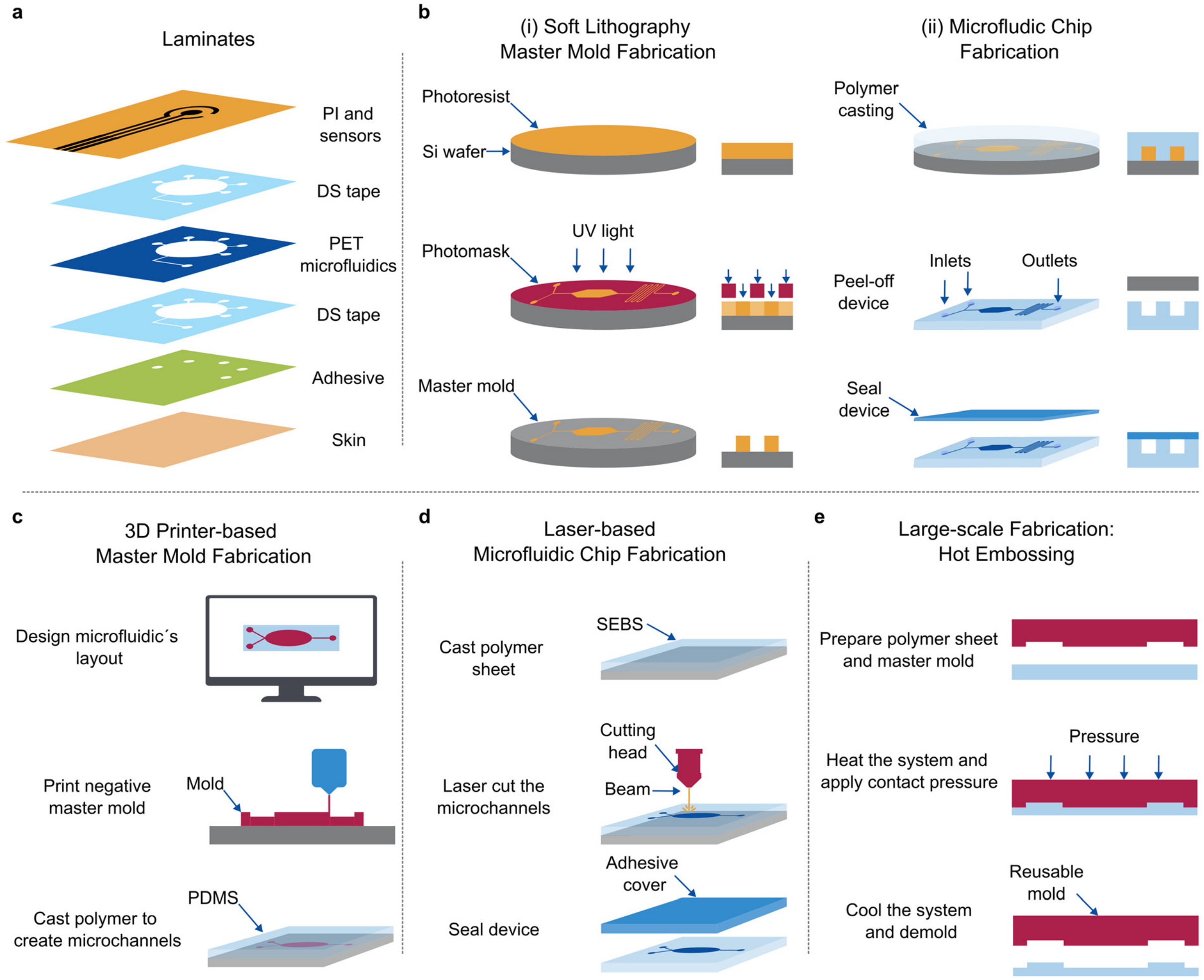

Fig. 7 Fabrication methods for microfluidic wearable biosensors. a) Laminate-based fabrication involves stacking layers from different materials to create the microchannels. PI: polyimide, DS: double-sided tape. b) Soft lithography is used to manufacture master molds for microfluidic fabrication. A polymer is cast on the mold surface and cured, transferring the master features to the polymeric substrate. c) 3D printing can be used to create the master molds avoiding the need for clean room access. However, this method's resolution depends on the printer and is generally low compared to other techniques. d) Laser-based fabrication uses different types of lasers to etch the microchannels into the substrate. This method can also be used to manufacture master molds. e) Hot embossing is a large-scale fabrication which uses a master mold and a thermoplastic to imprint the microfluidic design onto the polymer sheet.

polymer from the mold to avoid defects.[102] Furthermore, when choosing the material for mold fabrication, it is important to ensure low friction between the mold's material and the polymer to be cast. Also, chemical interactions between these materials should be taken into consideration.[87] It is recommended to treat the mold's surface to make it hydrophobic and facilitate polymer peeling off.[91] After removal, inlets and outlets can be defined by laser cutting or mechanical punching.[12]

Soft lithography can achieve structures from 20 μm to 100 μm. If smaller features are needed, advanced fabrication methods, such as e-beam lithography and two-photon polymerization, can be employed.[21] Other methods for mold creation involve micro-milling, laser ablation, and electron beam (e-beam) machining. However, they are generally more difficult to implement due to the need for specialized equipment.[87] Even though soft lithography has resolution limitations, the well-established protocols make it suited for wearable sensors.[47,98,99]

3D printing. 3D printing is an additive manufacturing technique where an object is created by adding successive layers of materials. Depending on the 3D printing equipment being used, the material is either a solid filament, or a resin cured under UV light.[87] This technique can be employed for manufacturing microfluidics in two different approaches. A 3D printer can print the mold where the polymer will be cast (Fig. 7c), or it can be used to print the layers of the microfluidic chip itself without the need to use external molds.[12]

This method can be combined with soft lithography to create complex 3D microfluidic structures. Shankles *et al.* propose a printing process for fabricating 3D bridge structures in polymer-based microfluidics.[75] The authors combined microchannel molds fabricated through conventional lithography techniques and 3D printing to fabricate the complete microfluidic chip. This allowed for the repurposing of microfabricated devices without the need for continuous cleanroom fabrication. In general, 3D printing is faster and more scalable than soft lithography; however, its resolution is lower and instrument-dependent.[12] However, when smaller features are needed, advanced 3D printing techniques such as two-photon photopolymerization can be used.[87]

One effective strategy to enhance the resolution of 3D-printed master molds is to combine additive and subtractive fabrication. In this hybrid approach, the initial structure is generated using 3D printing, and micro milling is subsequently employed to refine fine features. Micro milling relies on a high-precision rotating cutting tool, and when automated with computer numerical control (CNC), the process achieves high repeatability and improved dimensional accuracy.[103] Behroodi and colleagues demonstrated such a process by integrating projection micro-stereolithography with CNC micro milling, producing molds with significantly improved resolution and geometrical fidelity. Importantly, this combined method circumvents size limitations imposed by 3D printers alone, enabling the fabrication of large molds with microscale details.[104]

3D printing has been used in the development of several wearable devices. For example, Cho *et al.* studied the relationship between sweat and blood lactate for fitness applications.[105] They proposed a wearable band for time-dependent analysis of lactate and pH in sweat. This band consisted of several PDMS and PET layers for the creation of the microfluidics and sensing chambers. Bonding of the different layers was done through oxygen plasma treatment. The microchannels were patterned with a resin-based 3D printed mold and cast on PDMS.

Laser fabrication. Lasers are used for creating through holes, channels, and 3D microfluidic structures (Fig. 7d). The most common types of lasers are UV, femtosecond (fs), and CO_2 lasers; the choice of laser depends on the desired feature size and equipment capabilities.[87] There are different approaches to laser-based microfluidic fabrication. One of them is directly patterning the microchannels on the polymer surface. Waddell *et al.* proposed laser ablation on polymers for creating the microchannels and altering their surface chemistry.[106] They concluded that the most important laser parameters to control the depth of ablation are the rate at which the sample moves, the laser firing repetition rate, and the laser frequency. Furthermore, they experimented with cutting PMMA samples in different atmospheres (nitrogen, methanol, and water). Their experiments showed that ablation with nitrogen and methanol led to rectangular channel profiles, and ablation with water resulted in wedge-shaped profiles.

Besides direct microfluidic patterning, CO_2 lasers can be used to create electrochemical sensors on the flexible substrate. Yang *et al.* used a CO_2 laser to fabricate a wearable sensor to measure temperature, respiration rate, uric acid, and tyrosine in sweat.[107] Laser engraving was used to pattern the graphene-based electrochemical sensors and pattern the microfluidic channels on double-sided tape and PET. The system included 10 sweat inlets and was able to achieve a 90% sample refreshment in 2.5 minutes.

Another approach for microfluidic fabrication is using the laser to create a master mold. Saadat *et al.* proposed a rapid-prototyping protocol to create stainless steel molds using a femtosecond laser.[90] The laser was used to pattern the metal without the need for conventional photolithographic techniques. Furthermore, metallic molds can withstand higher curing temperatures and can be reused several times.

Large-scale fabrication. Large-scale fabrication methods are compatible with microfluidics made from thermoplastic materials such as polycarbonate (PC), PMMA, PET, and cyclic olefin copolymer (COC). The compatibility with different polymers makes them suitable for the development of microfluidics for wearable application.[108] There are several large-scale fabrication methods with injection molding, hot embossing, and roll-to-roll being the most common ones.

Injection molding is a high-throughput and cost-efficient microfluidic fabrication method. It involves the injection of a liquid state thermoplastic into a chamber containing the microfluidic mold, followed by its removal upon solidification.[102] Injection mold has several advantages, such as transferring of micro-scale features, replicability, automation, and availability of different thermoplastic materials. One of the drawbacks is the intense optimization of the process to ensure the polymer fills the mold cavity before solidification.[87]

Hot embossing involves placing a thermoplastic film between two mold inserts (Fig. 7e). The film is then compressed and heated to transfer the mold features.[102] As a general guideline, the hot embossing temperature must be higher than the plastic substrate's glass transition temperature.[89] When reaching high temperatures is not possible, the pressure can be elevated to imprint the design on the polymer film.[87]

Goral *et al.* developed a hot embossing method for rapid and small-scale prototyping of microfluidic chips.[89] The method used microscope glass slides, binder clips, and PDMS molds fabricated through soft lithography to emboss polystyrene substrates. The use of inexpensive materials and a low embossing temperature of 155 °C allows this method to be easily replicated in research-based environments.

Hot embossing fabrication can be combined with 3D printing for small-scale rapid prototyping of microfluidics. To this end, Khoo *et al.* proposed a protocol to fabricate thermoplastic microfluidic devices through 3D printed resin templates.[109] The general steps were as follows: first, the microfluidic device was designed and 3D printed. Then, a PDMS positive mold was created from the resin template. This mold was then used to cast an epoxy-based negative mold for hot embossing. The protocol needed intermediate steps for mold creation once the 3D printed resin was not able to be heated to the embossing temperatures. Even though extra fabrication steps were used, the authors demonstrated that their protocol can be completed in 48 hours at $15 per device.

Another promising technology for large-scale manufacturing, is roll-to-roll (R2R) processing. It has become one of the most widely adopted techniques for microfluidics. In this method, a flexible substrate, commonly paper or PET, is coated with the functional material and continuously fed between rollers equipped with a master mold. The microfluidic design is then thermally imprinted onto the substrate, producing patterned devices in a scalable and cost-efficient manner.[110–112] The main drawback of this technique lies in the high cost of fabricating the master mold, which typically requires cleanroom microfabrication. Boutiette *et al.* addressed this limitation by combining 3D printing for rapid master mold prototyping with R2R manufacturing for mass replication. This hybrid approach leverages the advantages of fast design iteration while avoiding the expense of traditional cleanroom processes, thereby making large-scale microfluidic production more accessible and adaptable.[113]

Choosing an appropriate microfluidic fabrication method will depend on the specific design goals, biofluid targets, and sensing applications (Table 5).

Laminate fabrication is accessible and fast to implement, while soft lithography remains the most popular technique for high-resolution microchannel design. Emerging methods such as 3D printing and laser-based fabrication offer alternatives for rapid iteration and integration. However, they are limited in resolution or material selection. Large-scale techniques like injection molding, hot embossing, and R2R can help researchers when transitioning from lab-based prototypes to clinical or commercial deployment. A clear understanding of these fabrication strategies is essential for selecting the most appropriate workflow when designing wearable microfluidics.

Future directions and emerging trends

The development of new microfluidic technologies becomes crucial as wearable biosensors continue to evolve from proof-of-concept prototypes to clinically relevant tools. Innovations in materials science, fabrication techniques, design strategies, and data analytics are expanding the capabilities of wearable microfluidic biosensors. These advancements not only improve the sensitivity, selectivity, and stability of wearable devices but also enable continuous, real-time monitoring of a broader range of biomarkers in non-invasive biofluids.

The next generation of microfluidic wearable biosensors will embrace emerging materials, open-source and collaborative platforms, and the use of artificial intelligence (AI) and machine learning (ML) for design and control. These advancements will allow for faster development of technology for sampling and manipulation of more biofluids, such as tears. This section explores the most promising future trends in the field to highlight where wearable microfluidic systems are heading in the next few years.

Even though polymers, specifically PDMS, are a popular material for fabricating microfluidics, they are not biodegradable and require extra treatments to make them hydrophilic. Hydrogels are a promising substitute. Their biocompatibility and hydrophilic properties make them ideal for the development of wearable biosensors.[114] However, they are prone to swelling, which makes them deform and lose mechanical stability. To address this problem, Shen *et al.* developed a non-swelling hydrogel-based microfluidic chip for cell and tissue applications.[115] Their protocol consisted of cross-linking a copolymer when fabricating the hydrogel; this fabrication procedure can be adapted to develop wearable microfluidics with enhanced biocompatibility.

Hydrogels have already been used in wearable microfluidic biosensors, as we previously discussed by the

Table 5 Comparison of the different fabrication methods for wearable microfluidic systems

Method	Key features	Advantages	Limitations	Feature resolution	Ref.
Laminates	Assembly of microfluidics layers *via* adhesives or thermal bonding	Rapid prototyping, material versatility, and scalability	Limited resolution, potential alignment issues	50–200 μm	28, 100–102
Soft lithography	Uses a master mold to cast and cure polymers with the desired geometry	Multilayer stacking, widely used, high-resolution features	Mold release challenges, moderate scalability, and cleanroom access may be needed for master mold fabrication	20–100 μm	21
3D printing	3D printing of microchannels or molds with filaments/resins	Fast iteration. Can print complex 3D structures or reusable master molds	Resolution is equipment-dependent	50–200 μm	75, 105
Laser fabrication	Laser ablation or engraving to pattern microchannels on flexible substrates	Direct write/patterning, material versatility, tunable depth control	Resolution is equipment-dependent, and thermal damage risk	20–200 μm	90, 106, 107
Large-scale methods	Injection molding, hot embossing, and roll-to-roll	High throughput, automation-ready, good reproducibility, wide range of feature sizes	Equipment-intensive, initial mold cost, only applicable to thermoplastics	5–200 μm	87, 89, 102

approach presented by. Lin *et al.* They exploit the hydrogel swelling property to create heat-controlled hydrogel valves for sweat flow control (Fig. 8a).[65] The use of electronically controlled microheaters allows for multiplexed and on-demand analyte detection. When the temperature goes above 45 °C, the hydrogels shrink, allowing sweat to flow towards the sensing chamber. Moreover, the system incorporates pressure release mechanisms to avoid breakage due to excess pressure from the sweat glands. To validate its functionality, the authors tested their device to detect glucose and lactate in sweat during exercise.

The design of microfluidics for non-experts becomes troublesome due to the extensive expertise and intuitive knowledge needed. Moreover, microfluidic construction usually requires several trial-and-error cycles, which can result in delays and increased costs. To this end, open-source online tools, where users can share their work and codes, including AI and ML algorithms, can be easily accessible, with a friendly interface allowing non-experts to design complex devices with optimized parameters without relying on the slow progress of trial and error. The main goal is to integrate these models into computer-aided design (CAD) software for a faster turnaround time. In the long term, it is expected that self-learning algorithms will allow the creation of smarter and more efficient microfluidics.[116,117]

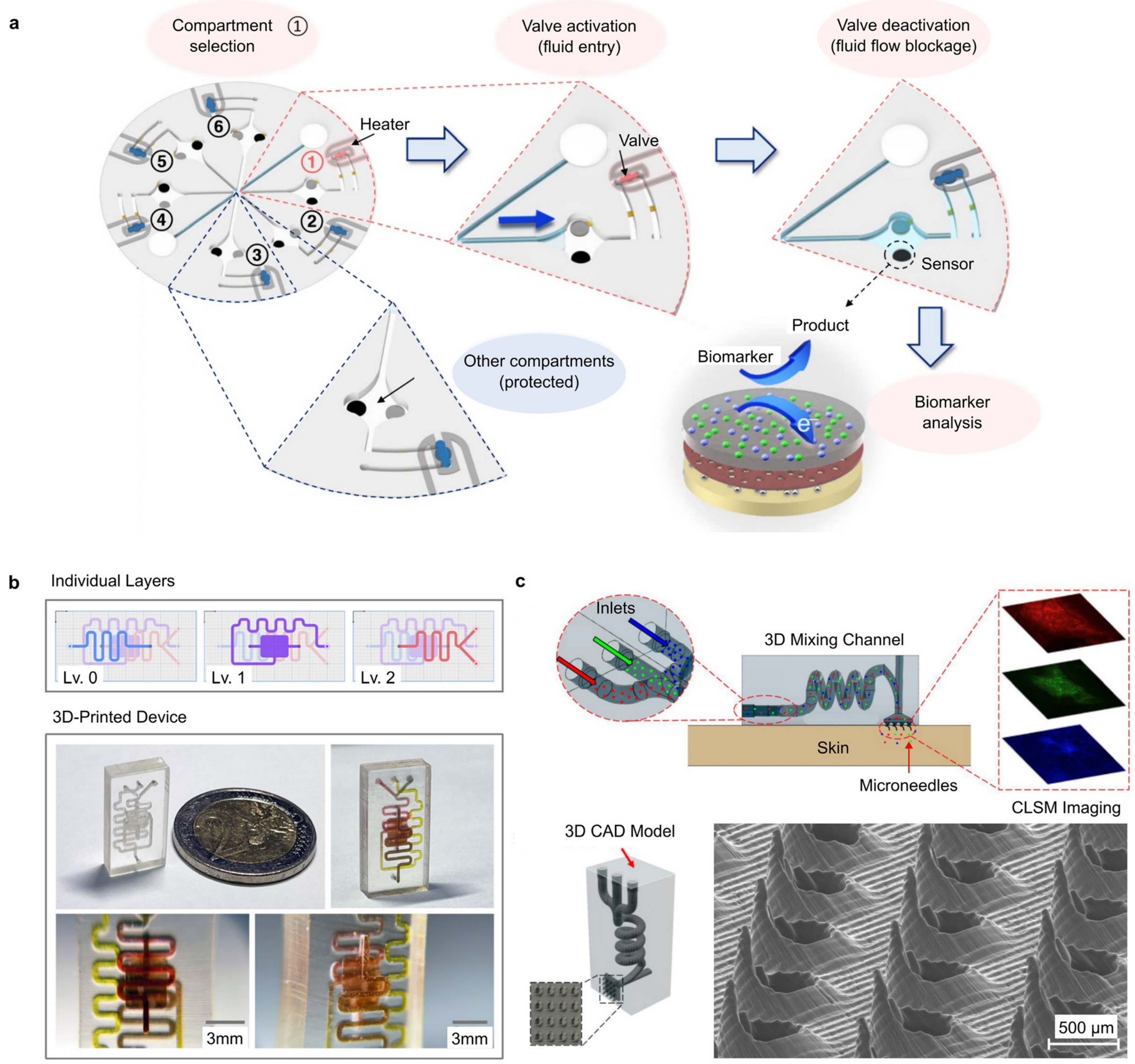

Fig. 8 Future trends in wearable microfluidics. a) Heat-controlled hydrogel valves for sweat flow control and multiplexed sensing.[65] b) Flui3d open-source microfluidic design CAD software and proof-of-concept 3D printed device.[119] c) 3D printed hollow microneedles and microfluidics for drug delivery.[129] [a) This figure has been adapted from ref. (65) with permission from Springer Nature, Copyright 2020; b) This figure has been adapted from ref. (119) with permission from Springer Nature, Copyright 2024; c) This figure has been adapted from ref. (129) with permission from AIP Publishing, Copyright 2019].

This review tutorial itself is a live example of the use of such open-source online tools. We made available a Jupyter Notebook with plug and play interface where anyone can design an optimized microfluidic design within seconds. Moreover, Nelson *et al.* proposed one of the first efforts to combine AI with CAD-based microfluidic design.[118] The authors utilized ChatGPT to generate microfluidic components in OpenSCAD, an open-source programming-based CAD software. GPT-4 was instructed to write the code for building a 3D (helix, valve, T-junction, and serpentine) and 2D (spiral and serpentine) microfluidic structures. Overall, the authors were able to create all structures using fewer than 14 prompts in approximately 1 hour per shape. For validation, all devices were 3D printed in resin and tested under flow. This study paves the way for the use of AI and CAD-based design. As algorithms advance, it will be possible to integrate such open-source AI models into more sophisticated software and designs.

Towards open-source design automation, Zhang *et al.* created Flui3d, a web-based platform for designing microfluidic chips for resin-based 3D printing (Fig. 8b).[119] Flui3d has a library of common microfluidic components and allows customized design of multi-layer fluidics. The main advantage is its design-for-manufacture (DFM) feature, which modifies the initial design to enhance its accuracy. The authors validated their tool with microfluidic devices from the literature in a commercial 3D resin-based printer. Even though they were able to print the devices successfully, Flui3d still needs a larger component library and application-based DFM rules.

Microfluidic design can be further automated with the aid of AI algorithms. Eijo and collaborators demonstrated a machine learning (ML) genetic algorithm capable of obtaining the optimal geometrical parameters for a capillary-driven microfluidic network based on the desired performance parameters.[120] Deep learning (DL) has been applied to the design of flow sculpting microfluidic devices, which arrange pillars inside the microchannel in a sequence such that the flow deforms as desired at the end of the channel. Stoecklein *et al.* proposed a convolutional neural network (CNN) for obtaining the design parameters of the flow sculpting device.[121] Both proven algorithms can be applied to the design of wearable devices when capillary-driven and passive flow control techniques are required.

The examples discussed so far have not been directly applied to wearable microfluidic design. Nevertheless, AI has already been integrated with wearable microfluidic devices for personalized diagnostics and treatment, primarily by leveraging its data analysis and decision-making capabilities.[13] Demonstrated applications include AI-assisted colorimetric detection of analytes in tears[57] and analysis of sweat and physiological biomarkers to assess stress responses.[122] Beyond data interpretation, AI has strong potential to aid in microfluidic design itself. As discussed, tools such as ML, DL, and GPT-4 have been demonstrated in the design of microfluidics. As an outlook, these same techniques have the potential to be applied to the design of high-throughput wearable microfluidics. For broader discussions on AI in microfluidics, including design automation, performance prediction, and system optimization, readers are referred to several recent comprehensive reviews.[13,116,123]

Advances in microfluidics materials, design, and fabrication will enable the use of more biofluids for wearable biosensors. Tears are a promising candidate due to a strong correlation with blood metabolite levels. The small volume of tears and limited space in the eyes make microfluidics essential in the development of tear-based wearables.[124] Contact lenses are one of the most popular tear-based biosensors. However, the fabrication of curved microfluidics becomes challenging. To address this, An *et al.* developed a fabrication method based on the irreversible bonding of PDMS and PET sheets.[125] The system takes advantage of the biocompatibility and established microchannel fabrication techniques for PDMS, and the ability of PET to be thermoformed to a curved shape. The authors were able to demonstrate microfluidics of features as small as 40 μm.

Moreover, contact lenses hold promise for closed-loop drug delivery systems for personalized therapeutics. Keum *et al.* designed a contact lens for electrochemical glucose monitoring and on-demand drug delivery for diabetic retinopathy.[126] The device included a wireless energy transfer system and electronics for sensing and wireless communication. This made drug delivery possible when a voltage was applied to the on-demand system. Although their contact lenses did not include microfluidic devices, the methodology can be used to integrate microfluidics for closed-loop tear-based drug delivery systems.

Besides tear-based microfluidic devices, microneedles and microfluidic integration hold great promise for sensing and drug delivery systems. This type of architecture is particularly important for ISF-based sensing. Microneedles can be functionalized with different biorecognition elements, including aptamers. This allows them to detect a wide range of analytes, from redox and non-redox active species.[127] Furthermore, fast and low-cost fabrication methods, such as 3D printing, can be used to develop microneedles.[128]

One example of 3D-printed hollow microneedles is described by Yeung *et al.*, where the authors combine microneedles and microfluidic fabrication in one step.[129] Their proposed system contains a 3D-printed microfluidic chip capable of mixing 3 reagents in different concentrations based on their flow rate (Fig. 8c). At the outlet of the device, the mixed reagents are injected into the skin. The authors tested different hollow needle architectures (conical, pyramidal, and fine-tip syringe-shaped), showing accuracy and repeatability through them.

From smart materials and AI-assisted design to open-source platforms and new biofluid targets, the future of this field lies in systems that are not only more functional and biocompatible but also more accessible and customizable. As research continues to bridge the gap between engineering innovation and real-world healthcare needs, wearable microfluidics can transform diagnostics and continuous health monitoring across diverse populations. Unlocking the full potential of these technologies will depend on interdisciplinary collaboration and a focus on usability and reliability of the proposed systems.

Conclusion and takeaways

Microfluidics for wearable biosensors have emerged as a disruptive technology that enables real-time, non-invasive health monitoring. Their successful integration requires the careful alignment of microfluidic design principles, material selection, fabrication strategies, and biofluid handling. This review has presented a tutorial-style framework that outlines the design process from fluid dynamics and channel geometry considerations to material and fabrication methods. By applying dimensional analysis and considering biofluid properties, researchers can engineer systems optimized for specific sensing needs and user contexts.

Material choice remains a critical factor in wearable microfluidics. Polymers like PDMS offer mechanical flexibility and compatibility with established fabrication methods, while paper substrates provide cost-effective platforms for disposable diagnostics. Hydrogels and other emerging materials present opportunities to improve biocompatibility and responsiveness. These choices must also account for the requirements and constraints of wearable systems, such as fluid interaction, sample purity, and user comfort.

Furthermore, advances in AI, CAD-based design, and open-source platforms are expanding accessibility and accelerating innovation. Integration of AI into the design pipeline offers a promising solution to the trial-and-error nature of microfluidic prototyping, allowing for rapid optimization and functional testing. As fabrication technologies continue to evolve, the scope of wearable microfluidic biosensing will broaden to include a wider range of biofluids, sensing modalities, and therapeutic applications.

Future efforts should focus on refining system integration, improving manufacturability, and ensuring long-term performance and reliability under real-world conditions. Interdisciplinary collaboration among engineers, clinicians, and data scientists will be essential to translate laboratory prototypes into clinically viable solutions. With a focus on usability, scalability, and robustness, wearable microfluidic systems can redefine personal health monitoring and pave the way for decentralized diagnostics.

Author contributions

J. Nava-Granados: writing – original draft, writing – review & editing, investigation, conceptualization, visualization. K. Vasquez: writing – original draft, investigation. B. U. Medina: writing – original draft, investigation, coding – idea, writing, & revision. C. Wang: writing – original draft, investigation. J. R. Moreto: writing – original draft, writing – review & editing, investigation, conceptualization, visualization, coding – idea, writing, & revision. J. Sempionatto: writing – original draft, writing – review & editing, investigation, conceptualization, visualization & funding acquisition.

Conflicts of interest

There are no conflicts to declare.

Data availability

The code for Microchannel Example Notebook can be found at https://colab.research.google.com/drive/1IO8TCqHDKW6L2ZaAvjEo3F7jYqOIH9ec?usp=sharing. The version of the code employed for this study is version 1.0.

Supplementary information: available with this review is an interactive Jupyter Notebook on Google Colab to help users begin designing wearable microfluidic systems. By selecting the target biofluid and device materials, the tool estimates key dimensions and fluidic parameters. See DOI: https://doi.org/10.1039/d5lc00628g.

Acknowledgements

J. N. G., K. V., and J. S. acknowledge the support from the startup grant at Rice University.

Notes and references

1 D. Xu, X. Huang, J. Guo and X. Ma, *Biosens. Bioelectron.*, 2018, **110**, 78–88.
2 D. G. Rackus, M. H. Shamsi and A. R. Wheeler, *Chem. Soc. Rev.*, 2015, **44**(15), 5320–5340.
3 S. Wang, X. Guan and S. Sun, *Sensors*, 2025, **25**(6), 1936.
4 T. M. Squires and S. R. Quake, *Rev. Mod. Phys.*, 2005, **77**(3), 977–1026.
5 V. Naresh and N. Lee, *Sensors*, 2021, **21**(4), 1109.
6 F. Pisapia, W. Balachandran and M. Rasekh, *Appl. Sci.*, 2022, **12**(8), 3829.
7 D. Dendukuri and P. S. Doyle, *Adv. Mater.*, 2009, **21**(41), 4071–4086.
8 B. Ramachandran and Y. C. Liao, *Biomicrofluidics*, 2022, **16**(5), 051501.
9 J. Kim, A. S. Campbell, B. E. F. de Ávila and J. Wang, *Nat. Biotechnol.*, 2019, **37**(4), 389–406.
10 K. Kuruvinashetti, A. Komeili and A. S. Nezhad, *Lab Chip*, 2025, **25**(16), 3879–3920.
11 S. R. S. Pour, D. Calabria, A. Emamiamin, E. Lazzarini, A. Pace, M. Guardigli, M. Zangheri and M. Mirasoli, *Biosensors*, 2024, **14**(1), 29.
12 S. Li, Z. Ma, Z. Cao, L. Pan and Y. Shi, *Small*, 2020, **16**(9), 1903822.
13 S. Apoorva, N. T. Nguyen and K. R. Sreejit, *Lab Chip*, 2024, **24**(7), 1833–1866.

14 E. Noviana, T. Ozer, C. S. Carrell, J. S. Link, C. McMahon, I. Jang and C. S. Henry, *Chem. Rev.*, 2021, **121**(19), 11835–11885.

15 L. L. Shen, G. R. Zhang and B. J. M. Etzold, *ChemElectroChem*, 2020, **7**(1), 10–30.

16 Z. Ye, Y. Yuan, S. Zhan, W. Liu, L. Fang and T. Li, *Analyst*, 2023, **148**(6), 1175–1188.

17 L. Bezinge, C. J. Shih, D. A. Richards and A. J. deMello, *Small*, 2024, **20**(38), 2401148.

18 S. Kumar, J. B. Kaushal and H. P. Lee, *Biosensors*, 2024, **14**(6), 300.

19 D. J. Harrison, K. Fluri, K. Seiler, Z. Fan, C. S. Effenhauser and A. Manz, *Science*, 1993, **261**(5123), 895–897.

20 A. Manz, N. Graber and H. M. Widmer, *Sens. Actuators, B*, 1990, **1**(1), 244–248.

21 J. C. McDonald, D. C. Duffy, J. R. Anderson, D. T. Chiu, H. Wu, O. J. A. Schueller and G. M. Whitesides, *Electrophoresis*, 2000, **21**(1), 27–40.

22 W. Gao, S. Emaminejad, H. Y. Y. Nyein, S. Challa, K. Chen, A. Peck, H. M. Fahad, H. Ota, H. Shiraki, D. Kiriya, D. Lien, G. A. Brooks, R. W. Davis and A. Javey, *Nature*, 2016, **529**(7587), 509–514.

23 B. Schazmann, D. Morris, C. Slater, S. Beirne, C. Fay, R. Reuveny, N. Moyna and D. Diamond, *Anal. Methods*, 2010, **2**(4), 342–348.

24 W. Jia, A. J. Bandodkar, G. Valdés-Ramírez, J. R. Windmiller, Z. Yang, J. Ramírez, G. Chan and J. Wang, *Anal. Chem.*, 2013, **85**(14), 6553–6560.

25 S. Coyle, K. T. Lau, N. Moyna, D. O'Gorman, D. Diamond, F. Di Francesco, D. Costanzo, P. Salvo, M. G. Trivella, D. E. De Rossi, N. Taccini, R. Paradiso, J.-A. Porchet, A. Ridolfi, J. Luprano, C. Chuzel, T. Lanier, F. Revol-Cavalier, S. Schoumacker, V. Mourier, I. Chartier, R. Convert, H. De-Moncuit and C. Bini, *IEEE Trans. Inf. Technol. Biomed.*, 2010, **14**(2), 364–370.

26 D. P. Rose, M. E. Ratterman, D. K. Griffin, L. Hou, N. Kelley-Loughnane and R. R. Naik, *IEEE Trans. Biomed. Eng.*, 2015, **62**(6), 1457–1465.

27 X. Huang, Y. Liu, K. Chen, W.-J. Shin, C.-J. Lu, G.-W. Kong, D. Patnaik, S.-H. Lee, J. F. Cortes and J. A. Rogers, *Small*, 2014, **10**(15), 3083–3090.

28 A. Koh, D. Kang, Y. Xue, S. Lee, R. M. Pielak, J. Kim, T. Hwang, S. Min, A. Banks, P. Bastien, M. C. Manco, L. Wang, K. R. Ammann, K.-I. Jang, P. Won, S. Han, R. Ghaffari, U. Paik, M. J. Slepian, G. Balooch, Y. Huang and J. A. Rogers, *Sci. Transl. Med.*, 2016, **8**(366), 366ra165.

29 J. Heikenfeld, *Electroanalysis*, 2016, **28**(6), 1242–1249.

30 J. Heikenfeld, A. Jajack, B. Feldman, S. W. Granger, S. Gaitonde, G. Begtrup and B. A. Katchman, *Nat. Biotechnol.*, 2019, **37**(4), 407–419.

31 H. Y. Y. Nyein, L.-C. Tai, Q. P. Ngo, M. Chao, G. B. Zhang, W. Gao, M. Bariya, J. Bullock, H. Kim, H. M. Fahad and A. Javey, *ACS Sens.*, 2018, **3**(5), 944–952.

32 T. R. Ray, J. Choi, A. J. Bandodkar, S. Krishnan, P. Gutruf, L. Tian, R. Ghaffari and J. A. Rogers, *Chem. Rev.*, 2019, **119**(8), 5461–5533.

33 J. Choi, Y. Xue, W. Xia, T. R. Ray, J. T. Reeder, A. J. Bandodkar, D. Kang, S. Xu, Y. Huang and J. A. Rogers, *Lab Chip*, 2017, **17**(15), 2572–2580.

34 A. J. Bandodkar, P. Gutruf, J. Choi, K. Lee, Y. Sekine, J. T. Reeder, W. J. Jeang, A. J. Aranyosi, S. P. Lee, J. B. Model, R. Ghaffari, C.-J. Su, J. P. Leshock, T. Ray, A. Verrillo, K. Thomas, V. Krishnamurthi, S. Han, J. Kim, S. Krishnan, T. Hang and J. A. Rogers, *Sci. Adv.*, 2019, **5**(1), eaav3294.

35 L. B. Baker, J. B. Model, K. A. Barnes, M. L. Anderson, S. P. Lee, K. A. Lee, S. D. Brown, A. J. Reimel, T. J. Roberts, R. P. Nuccio, J. L. Bonsignore, C. T. Ungaro, J. M. Carter, W. Li, M. S. Seib, J. T. Reeder, A. J. Aranyosi, J. A. Rogers and R. Ghaffari, *Sci. Adv.*, 2020, **6**(50), eabe3929.

36 N. T. Nguyen and S. T. Wereley, *Fundamentals and applications of microfluidics*, Artech House, 2006.

37 S. F. Berlanda, M. Breitfeld, C. L. Dietsche and P. S. Dittrich, *Anal. Chem.*, 2021, **93**(1), 311–331.

38 N. Convery and N. Gadegaard, *Micro Nano Eng.*, 2019, **2**, 76–91.

39 H. Bruus, *Theoretical microfluidics*, Oxford Univ. Press, 2011.

40 F. M. White, *Fluid Mechanics*, McGraw-Hill, 2011.

41 Y. A. Çengel and J. M. Cimbala, *Fluid Mechanics: Fundamentals and Applications*, McGraw-Hill Education, 2017.

42 P. Kundu, I. Cohen and D. Dowling, *Fluid Mechanics*, Elsevier, 2016.

43 F. M. White and J. Majdalani, *Viscous Fluid Flow*, McGraw-Hill, 2022.

44 R. L. Panton, *Incompressible Flow*, John Wiley & Sons, Inc., 2013.

45 A. L. Gerhart, J. I. Hochstein and P. M. Gerhart, *Fundamentals of fluid mechanics*, Wiley, 2020.

46 G. M. Whitesides, *Nature*, 2006, **442**(7101), 368–373.

47 A. Martín, J. Kim, J. F. Kurniawan, J. R. Sempionatto, J. R. Moreto, G. Tang, A. S. Campbell, A. Shin, M. Y. Lee, X. Liu and J. Wang, *ACS Sens.*, 2017, **2**(12), 1860–1868.

48 J. Choi, D. Kang, S. Han, S. B. Kim and J. A. Rogers, *Adv. Healthcare Mater.*, 2017, **6**(5), 1601355.

49 C. Ye, M. Wang, J. Min, R. Y. Tay, H. Lukas, J. R. Sempionatto, J. Li, C. Xu and W. Gao, *Nat. Nanotechnol.*, 2024, **19**(3), 330–337.

50 S. Wang, X. Zhang, C. Ma, S. Yan, D. Inglis and S. Feng, *Biosensors*, 2021, **11**(10), 405.

51 G. Gharib, İ. Bütün, Z. Muganlı, G. Kozalak, İ. Namlı, S. S. Sarraf, V. E. Ahmadi, E. Toyran, A. J. van Wijnen and A. Koşar, *Biosensors*, 2022, **12**(11), 1023.

52 Y. Song, Y. Zhou, K. Zhang, Z. Fan, F. Zhang and M. Wei, *Lab Chip*, 2024, **24**(19), 4483–4513.

53 A. Olanrewaju, M. Beaugrand, M. Yafia and D. Juncker, *Lab Chip*, 2018, **18**(16), 2323–2347.

54 A. P. Iakovlev, A. S. Erofeev and P. V. Gorelkin, *Biosensors*, 2022, **12**(11), 956.

55 T. Saha, S. Mukherjee, M. D. Dickey and O. D. Velev, *Lab Chip*, 2024, **24**(5), 1244–1265.

56 J. Xu, X. Tao, X. Liu and L. Yang, *Anal. Chem.*, 2022, **94**(24), 8659–8667.

57 Z. Wang, Y. Dong, X. Sui, X. Shao, K. Li, H. Zhang, Z. Xu and D. Zhang, *npj Flexible Electron.*, 2024, **8**(1), 35.

58 D. J. O'Brien, D. Mills, J. Farina and M. Paranjape, *IEEE Trans. Biomed. Eng.*, 2023, **70**(9), 2573–2580.

59 J. Xiao, S. Zhang, Q. Liu, T. Xu and X. Zhang, *Sens. Actuators, B*, 2024, **398**, 134685.

60 Y. Zheng, H. Shi, Z. Tan, W. Xu, Z. Dan, J. Liao, Z. Dai, N. M. Reis, D. Wu and Z. Liu, *Chem. Eng. J.*, 2025, **519**, 165007.

61 H. Y. Y. Nyein, M. Bariya, B. Tran, C. H. Ahn, B. J. Brown, W. Ji, N. Davis and A. Javey, *Nat. Commun.*, 2021, **12**(1), 1823.

62 P. H. Lin, W. L. Chang, S. C. Sheu and B. R. Li, *iScience*, 2020, **23**(11), 101658.

63 I. J. Schulz, *J. Clin. Invest.*, 1969, **48**(8), 1470–1477.

64 J. R. Sempionatto, J. A. Lasalde-Ramírez, K. Mahato, J. Wang and W. Gao, *Nat. Rev. Chem.*, 2022, **6**(12), 899–915.

65 H. Lin, J. Tan, J. Zhu, S. Lin, Y. Zhao, W. Yu, H. Hojaiji, B. Wang, S. Yang, X. Cheng, Z. Wang, E. Tang, C. Yeung and S. Emaminejad, *Nat. Commun.*, 2020, **11**(1), 4405.

66 J. R. Sempionatto, L. Canniatti Brazaca, L. García-Carmona, G. Bolat, A. S. Campbell, A. Martin, E. S. Gonzalez and J. Wang, *Biosens. Bioelectron.*, 2019, **137**, 161–170.

67 Y. Han, X. Fang, H. Li, L. Zha, J. Guo and X. Zhang, *ACS Sens.*, 2023, **8**(12), 4774–4781.

68 Y. Cheng, S. Feng, Q. Ning, T. Li, H. Xu, Q. Sun, D. Cui and K. Wang, *Microsyst. Nanoeng.*, 2023, **9**(1), 36.

69 A. M. Nightingale, C. L. Leong, R. A. Burnish, S.-u. Hassan, Y. Zhang, G. F. Clough, M. G. Boutelle, D. Voegeli and X. Niu, *Nat. Commun.*, 2019, **10**(1), 2741.

70 B. Mayol, I. Z. Qubbaj, J. Nava-Granados, K. Vasquez, S. T. Keene and J. R. Sempionatto, *Biosensors*, 2025, **15**(5), 277.

71 A. Hauke, P. Simmers, Y. R. Ojha, B. D. Cameron, R. Ballweg, T. Zhang, N. Twine, M. Brothers, E. Gomez and J. Heikenfeld, *Lab Chip*, 2018, **18**(24), 3750–3759.

72 R. Peng, Z. Sonner, A. Hauke, E. Wilder, J. Kasting, T. Gaillard, D. Swaille, F. Sherman, X. Mao, J. Hagen, R. Murdock and J. Heikenfeld, *Lab Chip*, 2016, **16**(22), 4415–4423.

73 H. Y. Y. Nyein, M. Bariya, L. Kivimäki, S. Uusitalo, T. S. Liaw, E. Jansson, C. H. Ahn, J. A. Hangasky, J. Zhao, Y. Lin, T. Happonen, M. Chao, C. Liedert, Y. Zhao, L.-C. Tai, J. Hiltunen and A. Javey, *Sci. Adv.*, 2019, **5**(8), eaaw9906.

74 I. Miranda, A. Souza, P. Sousa, J. Ribeiro, E. M. S. Castanheira, R. Lima and G. Minas, *J. Funct. Biomater.*, 2022, **13**(1), 2.

75 P. G. Shankles, L. J. Millet, J. A. Aufrecht and S. T. Retterer, *PLoS One*, 2018, **13**(3), e0192752.

76 G. Bolat, E. De la Paz, N. F. Azeredo, M. Kartolo, J. Kim, A. N. de Loyola E Silva, R. Rueda, C. Brown, L. Angnes, J. Wang and J. R. Sempionatto, *Anal. Bioanal. Chem.*, 2022, **414**(18), 5411–5421.

77 R. E. Johnson, F. Sargent, F. Robbins, T. Morimoto, K. Shil Shin, B. Blase, S. Kinney, M. Brookens, J. Harris, D. Wakat, P. Mole, W. Kachadorian, J. Nelson, G. Benner and J. Davis, *The Physical and Chemical Properties of Human Sweat and Factors Affecting the Water Balance in Confined Space*, University of Illinois, 1966.

78 W. Yao, Y. Li and G. Ding, *Evid. Based Complement. Alternat. Med.*, 2012, **2012**(1), 853516.

79 M. Beigtan, M. Gonçalves and B. M. Weon, *Environ. Sci. Technol.*, 2024, **58**(15), 6532–6539.

80 L. Li, R. J. Braun, K. L. Maki, W. D. Henshaw and P. E. King-Smith, *Phys. Fluids*, 2014, **26**(5), 052101.

81 B. Nagyová and J. M. Tiffany, *Curr. Eye Res.*, 1999, **19**(1), 4–11.

82 S. Gittings, N. Turnbull, B. Henry, C. J. Roberts and P. Gershkovich, *Eur. J. Pharm. Biopharm.*, 2015, **91**, 16–24.

83 J. P. Kirkness, T. C. Amis, J. R. Wheatley and H. K. Christenson, *J. Colloid Interface Sci.*, 2000, **232**(2), 408–409.

84 A. J. M. Ligtenberg, M. Meuffels and E. C. I. Veerman, *Arch. Oral Biol.*, 2020, **109**, 104593.

85 E. Kubala, P. Strzelecka, M. Grzegocka, D. Lietz-Kijak, H. Gronwald, P. Skomro and E. Kijak, *BioMed Res. Int.*, 2018, **2018**(1), 6572381.

86 R. F. R. Ursem, A. Steijlen, M. Parrilla, J. Bastemeijer, A. Bossche and K. D. Wael, *Lab Chip*, 2025, **6**(17), eaba3252.

87 S. M. Scott and Z. Ali, *Micromachines*, 2021, **12**(3), 319.

88 H. Joodaki and M. B. Panzer, *Proc. Inst. Mech. Eng., Part H*, 2018, **232**(4), 323–343.

89 V. N. Goral, Y. C. Hsieh, O. N. Petzold, R. A. Faris and P. K. Yuen, *J. Micromech. Microeng.*, 2010, **21**(1), 017002.

90 M. Saadat, M. Taylor, A. Hughes and A. M. Hajiyavand, *Adv. Mech. Eng.*, 2020, **12**(12), 1687814020982713.

91 A. Shakeri, S. Khan and T. F. Didar, *Lab Chip*, 2021, **21**(16), 3053–3075.

92 N. B. Twine, R. M. Norton, M. C. Brothers, A. Hauke, E. F. Gomez and J. Heikenfeld, *Lab Chip*, 2018, **18**(18), 2816–2825.

93 A. K. Yetisen, M. S. Akram and C. R. Lowe, *Lab Chip*, 2013, **13**(12), 2210–2251.

94 R. Ghosh, S. Gopalakrishnan, R. Savitha, T. Renganathan and S. Pushpavanam, *Sci. Rep.*, 2019, **9**(1), 7896.

95 U. Mogera, H. Guo, M. Namkoong, M. S. Rahman, T. Nguyen and L. Tian, *Sci. Adv.*, 2022, **8**(12), eabn1736.

96 M. Parrilla, T. Guinovart, J. Ferré, P. Blondeau and F. J. Andrade, *Adv. Healthcare Mater.*, 2019, **8**(16), 1900342.

97 L. F. de Castro, S. V. de Freitas, L. C. Duarte, J. A. C. de Souza, T. R. L. C. Paixão and W. K. T. Coltro, *Anal. Bioanal. Chem.*, 2019, **411**(19), 4919–4928.

98 D. Liu, Z. Liu, S. Feng, Z. Gao, R. Chen, G. Cai and S. Bian, *Biosensors*, 2023, **13**(2), 157.

99 L. Yin, M. Cao, K. N. Kim, M. Lin, J.-M. Moon, J. R. Sempionatto, J. Yu, R. Liu, C. Wicker, A. Trifonov, F. Zhang, H. Hu, J. R. Moreto, J. Go, S. Xu and J. Wang, *Nat. Electron.*, 2022, **5**(10), 694–705.

100 M. Wang, Y. Yang, J. Min, Y. Song, J. Tu, D. Mukasa, C. Ye, C. Xu, N. Heflin, J. S. McCune, T. K. Hsiai, Z. Li and W. Gao, *Nat. Biomed. Eng.*, 2022, **6**(11), 1225–1235.

101 T. Sun, J. Hui, L. Zhou, B. Lin, H. Sun, Y. Bai, J. Zhao and H. Mao, *Sens. Actuators, B*, 2022, **368**, 132184.

102 B. K. Gale, A. R. Jafek, C. J. Lambert, B. L. Goenner, H. Moghimifam, U. C. Nze and S. K. Kamarapu, *Inventions*, 2018, **3**(3), 60.

103 D. J. Guckenberger, T. E. de Groot, A. M. D. Wan, D. J. Beebe and E. W. K. Young, *Lab Chip*, 2015, **15**(11), 2364–2378.

104 E. Behroodi, H. Latifi, Z. Bagheri, E. Ermis, S. Roshani and M. S. Moghaddam, *Sci. Rep.*, 2020, **10**(1), 22171.

105 S. Cho, S. M. Shaban, R. Song, H. Zhang, D. Yang, M.-J. Kim, Y. Xiong, X. Li, K. Madsen, S. Wapnick, S. Zhang, Z. Chen, J. Kim, G. Guinto, M. Li, M. Lee, R. F. Nuxoll, S. Shajari, J. Wang, S. Son, J. Shin, A. J. Aranyosi, D. E. Wright, T.-I. Kim, R. Ghaffari, Y. Huang, D.-H. Kim and J. A. Rogers, *Sci. Transl. Med.*, 2024, **16**(763), eado5366.

106 E. A. Waddell, L. E. Locascio and G. W. Kramer, *JALA*, 2002, **7**(1), 78–82.

107 Y. Yang, Y. Song, X. Bo, J. Min, O. S. Pak, L. Zhu, M. Wang, J. Tu, A. Kogan, H. Zhang, T. K. Hsiai, Z. Li and W. Gao, *Nat. Biotechnol.*, 2020, **38**(2), 217–224.

108 N. Kashaninejad and N. T. Nguyen, *Lab Chip*, 2023, **23**(5), 913–937.

109 H. Khoo, W. S. Allen, N. Arroyo-Currás and S. C. Hur, *Sci. Rep.*, 2024, **14**(1), 1–11.

110 S. H. Ahn and L. J. Guo, *ACS Nano*, 2009, **3**(8), 2304–2310.

111 J. Hiltunen, C. Liedert, M. Hiltunen, O.-H. Huttunen, J. Hiitola-Keinänen, S. Aikio, M. Harjanne, M. Kurkinen, L. Hakalahti and L. P. Lee, *Lab Chip*, 2018, **18**(11), 1552–1559.

112 M. Bariya, Z. Shahpar, H. Park, J. Sun, Y. Jung, W. Gao, H. Y. Y. Nyein, T. S. Liaw, L.-C. Tai, Q. P. Ngo, M. Chao, Y. Zhao, M. Hettick, G. Cho and A. Javey, *ACS Nano*, 2018, **12**(7), 6978–6987.

113 A. L. Boutiette, C. Toothaker, B. Corless, C. Boukaftane and C. Howell, *PLoS One*, 2020, **15**(12), e0244324.

114 X. Zhang, L. Li and C. Luo, *Lab Chip*, 2016, **16**(10), 1757–1776.

115 C. Shen, Y. Li, Y. Wang and Q. Meng, *Lab Chip*, 2019, **19**(23), 3962–3973.

116 D. McIntyre, A. Lashkaripour, P. Fordyce and D. Densmore, *Lab Chip*, 2022, **22**(16), 2925–2937.

117 K. Goda, H. Lu, P. Fei and J. Guck, *Lab Chip*, 2023, **23**(17), 3737–3740.

118 M. D. Nelson, B. L. Goenner and B. K. Gale, *Lab Chip*, 2023, **23**(17), 3778–3784.

119 Y. Zhang, M. Li, T. M. Tseng and U. Schlichtmann, *Commun. Eng.*, 2024, **3**(1), 71.

120 P. M. G. Eijo, T. Duriez, J. M. Cabaleiro and G. Artana, *Lab Chip*, 2022, **22**(24), 4860–4870.

121 D. Stoecklein, L. G. Lore, M. Davies, S. Sarkar and B. Ganapathysubramanian, *Sci. Rep.*, 2017, **7**(1), 46368.

122 C. Xu, Y. Song, J. R. Sempionatto, S. A. Solomon, Y. Yu, H. Y. Y. Nyein, R. Y. Tay, J. Li, W. Heng, J. Min, A. Lao, T. K. Hsiai, J. A. Sumner and W. Gao, *Nat. Electron.*, 2024, **7**(2), 168–179.

123 J. Zhou, J. Dong, H. Hou, L. Huang and J. Li, *Lab Chip*, 2024, **24**(5), 1307–1326.

124 M. A. Aravind, A. Saxena, D. Mishra, K. Singh and S. D. George, *Microsyst. Nanoeng.*, 2025, **11**(1), 1–16.

125 H. An, L. Chen, X. Liu, B. Zhao, D. Ma and Z. Wu, *J. Micromech. Microeng.*, 2018, **28**(10), 105008.

126 D. H. Keum, S.-K. Kim, J. Koo, G.-H. Lee, C. Jeon, J. W. Mok, B. H. Mun, K. J. Lee, E. Kamrani, C.-K. Joo, S. Shin, J.-Y. Sim, D. Myung, S. H. Yun, Z. Bao and S. K. Hahn, *Sci. Adv.*, 2020, **6**(17), eaba3252.

127 Y. Wu, F. Tehrani, H. Teymourian, J. Mack, A. Shaver, M. Reynoso, J. Kavner, N. Huang, A. Furmidge, A. Duvvuri, Y. Nie, L. M. Laffel, F. J. Doyle III, M.-E. Patti, E. Dassau, J. Wang and N. Arroyo-Currás, *Anal. Chem.*, 2022, **94**(23), 8335–8345.

128 M. Reynoso, A. Y. Chang, Y. Wu, R. Murray, S. Suresh, Y. Dugas, J. Wang and N. Arroyo-Currás, *Biosens. Bioelectron.*, 2024, **244**, 115802.

129 C. Yeung, S. Chen, B. King, H. Lin, K. King, F. Akhtar, G. Diaz, B. Wang, J. Zhu, W. Sun, A. Khademhosseini and S. Emaminejad, *Biomicrofluidics*, 2019, **13**(6), 064125.